

Article

Familial Alzheimer's Disease Neurons Bearing Mutations in *PSEN1* Display Increased Calcium Responses to AMPA as an Early Calcium Dysregulation Phenotype

Helena Targa Dias Anastacio ¹, Natalie Matosin ² and Lezanne Ooi ^{1,*}

¹ Molecular Horizons and School of Chemistry and Molecular Bioscience, University of Wollongong, Northfields Avenue, Wollongong, NSW 2522, Australia; htada204@uowmail.edu.au

² School of Medical Sciences, Faculty of Medicine and Health, The University of Sydney, Sydney, NSW 2050, Australia; natalie.matosin@sydney.edu.au

* Correspondence: lezanne@uow.edu.au; Tel.: +61-2-42215865

Abstract: Familial Alzheimer's disease (FAD) can be caused by mutations in *PSEN1* that encode presenilin-1, a component of the gamma-secretase complex that cleaves amyloid precursor protein. Alterations in calcium (Ca^{2+}) homeostasis and glutamate signaling are implicated in the pathogenesis of FAD; however, it has been difficult to assess in humans whether or not these phenotypes are the result of amyloid or tau pathology. This study aimed to assess the early calcium and glutamate phenotypes of FAD by measuring the Ca^{2+} response of induced pluripotent stem cell (iPSC)-derived neurons bearing *PSEN1* mutations to glutamate and the ionotropic glutamate receptor agonists NMDA, AMPA, and kainate compared to isogenic control and healthy lines. The data show that in early neurons, even in the absence of amyloid and tau phenotypes, FAD neurons exhibit increased Ca^{2+} responses to glutamate and AMPA, but not NMDA or kainate. Together, this suggests that *PSEN1* mutations alter Ca^{2+} and glutamate signaling as an early phenotype of FAD.

Keywords: Alzheimer's disease; induced pluripotent stem cells; neurodegeneration; AMPA; glutamate



Citation: Targa Dias Anastacio, H.; Matosin, N.; Ooi, L. Familial Alzheimer's Disease Neurons Bearing Mutations in *PSEN1* Display Increased Calcium Responses to AMPA as an Early Calcium Dysregulation Phenotype. *Life* **2024**, *14*, 625. <https://doi.org/10.3390/life14050625>

Academic Editors: Andres Daniel Maturana and Carlo Musio

Received: 28 February 2024

Revised: 18 April 2024

Accepted: 8 May 2024

Published: 12 May 2024



Copyright: © 2024 by the authors. Licensee MDPI, Basel, Switzerland. This article is an open access article distributed under the terms and conditions of the Creative Commons Attribution (CC BY) license (<https://creativecommons.org/licenses/by/4.0/>).

1. Introduction

Alzheimer's disease (AD) is the most common neurodegenerative disorder in the world, with memory loss and cognitive dysfunction being common symptoms. The majority of cases are termed sporadic, caused by a combination of genetic and environmental factors, while less than 2% of cases are termed familial Alzheimer's disease (FAD) [1], caused by mutations in one of three genes: *PSEN1*, *PSEN2*, or *APP*, which each play a role in the generation of amyloid- β peptides [2]. Amyloid- β plaques in the extracellular space [3] and hyperphosphorylated tau in neurons [4] are two of the hallmarks of the disease. Current treatments available alleviate behavioral symptoms but do not stop neuronal degeneration. Hence, there is a great need to identify early pathways altered by the disease.

Calcium (Ca^{2+}) dyshomeostasis is implicated in the pathogenesis of AD [5,6]. Several studies have reported mutations in the presenilin genes that alter intracellular Ca^{2+} levels by modifying endoplasmic reticulum (ER) and lysosomal Ca^{2+} release [7–11]. Apart from Ca^{2+} release from intracellular stores, the elevation of cytosolic Ca^{2+} concentration can occur through the influx of extracellular Ca^{2+} . The activation of glutamate receptors is a major source of Ca^{2+} influx [5]. Glutamate is the most abundant excitatory neurotransmitter in the mammalian central nervous system, and it mediates excitatory synaptic transmission via activation of ionotropic (iGluRs) and metabotropic (mGluRs) glutamate receptors in the post-synaptic membrane. Ionotropic receptors are ligand-gated ion channels that mediate excitatory synaptic transmission via the influx of Na^+ and Ca^{2+} into the cytoplasm. They are divided into 3 groups: α -amino-3-hydroxy-5-methyl-4-isoaxazolepropionic acid (AMPA), *N*-methyl-d-aspartate (NMDA), and kainate (KA) receptors [12]. AMPARs are composed

of a combination of four subunits (GluA1–GluA4). In the rodent cortex, GluA1 comprises almost 50% of all AMPAR subunits, followed by similar levels of GluA2 and GluA3 [13]. Soluble oligomeric A β binds to AMPARs and promotes their internalization, leading to depressed synaptic transmission [14]. However, contrasting results have also found that A β increases expression of synaptic AMPAR, increasing synaptic transmission [15]. Hyperphosphorylated tau mislocalised to dendritic spines also disrupts synaptic function by dysregulating AMPAR trafficking [16]. NMDARs have seven different subunits: one GluN1, four GluN2 (GluN2A, GluN2B, GluN2C, and GluN2D), and two GluN3 subunits (GluN3A and GluN3B). Functional NMDARs are heterotetramers composed of two GluN1 and two GluN2 or GluN3 subunits [17]. Activation of extrasynaptic NMDARs increases production of tau [18] and A β [19,20]. In turn, amyloid- β increases extrasynaptic NMDAR activation by decreasing neuronal glutamate uptake [21–23], but it can also promote NMDAR endocytosis, causing synaptic depression [24]. The NMDAR antagonist memantine is used to treat moderate to severe cases of AD [25], thus targeting NMDA signalling can address some of the symptoms of AD. Kainate receptors (KAR) are composed of a tetrameric assembly of subunits GluK1–5. These receptors are strongly implicated in epilepsy and seizures [26], but little is known about their role in AD. Recent work, however, has found decreased protein expression of the GluK2 subunit and impaired KAR-mediated synaptic transmission in a mouse model of AD [27]. The function and expression of iGluRs play an important role in regulating synaptic plasticity. Through this property, neurons can modulate synaptic strength in response to the intensity and duration of a synaptic input, which is thought to underlie the formation of memory [28]. However, the majority of studies in human *postmortem* brain tissue have shown reduced expression of AMPAR, NMDAR, and KAR at the end stages of the disease, as summarised in [29].

Even though glutamatergic neurotransmission is required for synaptic plasticity, excessive activation of excitatory receptors results in excitotoxicity, whereby an elevated influx of Ca²⁺ initiates a signalling cascade that promotes cell death [30]. Hence, glutamatergic stimuli and levels of intracellular Ca²⁺ need to be tightly regulated in order to promote synaptic plasticity and avoid neuronal damage. However, a range of evidence suggests there is significant disruption to Ca²⁺ homeostasis, hyperactive (increased activity of) glutamatergic signalling, and neuronal excitability in AD. (1) Studies using different transgenic animal models expressing mutant *APP*, *PSEN*, and/or *MAPT* genes to model AD pathogenesis have detected elevated basal and stimulus-evoked glutamate release in the entorhinal cortex, dentate gyrus, CA1, and CA3 regions of the hippocampus [31]. (2) Concurrently, various studies have found neuronal hyperactivity in animal and cell models of AD, as well as in patients in the early stages of AD [32]. (3) Clinical studies have also detected a hyperactive phenotype of cortical and hippocampal brain regions in individuals at risk of developing AD, while brain hypoactivity was observed at later stages of the disease [33,34]. (4) Similar abnormalities have been detected in animal and cell models of AD, in which neurons displayed elevated Ca²⁺ signals and increased excitability [35–38]. Cell studies using induced pluripotent stem cells (iPSCs) from AD patients comprise a smaller fraction of research on neuronal excitability changes in AD but represent a useful tool to assess human cells and the impact of FAD-causing mutations compared to isogenic control lines.

Altogether, the current literature has identified numerous abnormalities in Ca²⁺ signalling and glutamatergic transmission in AD. Here, we aimed to assess the early calcium phenotypes of FAD neurons to identify whether these may precede AD pathology. In particular, we aimed to quantify differences in the magnitude of Ca²⁺ responses to iGluR agonists in early neurons representing FAD patients. Thus, we treated iPSC-derived excitatory cortical neurons from FAD patients, isogenic controls, and healthy individuals with glutamate, NMDA, AMPA, and kainate and measured the associated Ca²⁺ responses to determine the impact of iGluR agonists on the calcium phenotype in FAD neurons. Our data shows that FAD neurons demonstrate increased calcium responses to AMPA, even in the absence of amyloid and tau phenotypes, highlighting an early phenotype in FAD neurons that may contribute to calcium dysregulation.

2. Materials and Methods

2.1. Cell Culture and Neuronal Differentiation: Induced Pluripotent Stem Cell Culture

The induced pluripotent stem cell lines used in this study are described in Table 1. All cell lines were checked for karyotype abnormalities, RNA and protein expression of pluripotency markers, ability to differentiate into 3 germ layers, STR profiling, and genomic DNA sequencing. Experiments using human-derived iPSCs were approved by the University of Wollongong Human Ethics Committee and conducted in accordance with HE13/299 (Wollongong, Australia). To establish iPSCs from frozen stocks, cells were thawed at 37 °C in a water bath and mixed with warm DMEM/F12 medium. The cells were centrifuged for 5 min at 300 × *g*, the supernatant was aspirated, and the pellet was resuspended in mTeSR1 (Stem Cell Technologies; Vancouver, BC, Canada) medium. Colonies were then plated into a 60 mm tissue culture dish coated with 0.1 mg/mL Matrigel (Corning; Corning, NY, USA), fed with mTeSR1, and kept in a humidified incubator at 37 °C with 5% CO₂ and 3% O₂. The medium was changed every day, and spontaneously differentiated cells were manually removed using a sterile pipette tip. Colonies were passaged every 5–7 days with Mg²⁺/Ca²⁺-free Phosphate Buffered Saline (PBS) (Thermo Fisher Scientific; Waltham, MA, USA) with 0.5 mM Ethylenediaminetetraacetic acid (EDTA; Life Technologies; Carlsbad, CA, USA) (PBS/EDTA). After 3–5 min in PBS-EDTA, colonies were detached by flushing DMEM/F12 into the dish. The medium containing the cells was then transferred into a centrifuge tube and centrifuged for 5 min at 300 × *g*. The supernatant was discarded, and colonies were resuspended in 1 mL of mTeSR1 before being plated on a new Matrigel-coated dish.

Table 1. Details of induced pluripotent cell lines.

iPSC Name	Disease Status	WT/Mutation	APOE Genotype	Age at Collection	Sex	iPSC Line Characterisation
FAD1	Familial AD	<i>PSEN1</i> ^{S290C}	ε3/3	47	M	[39]
IC1	Isogenic control	<i>PSEN1</i> ^{WT}	ε3/3	47	M	[39]
HC1	Healthy control	<i>PSEN1</i> ^{WT}	ε2/4	57	F	[40]
FAD2	Familial AD	<i>PSEN1</i> ^{A246E}	ε3/4	56	F	[41]
IC2	Isogenic control	<i>PSEN1</i> ^{WT}	ε3/4	56	F	Anastacio et al., 2024 in revision
HC2	Healthy control	<i>PSEN1</i> ^{WT}	ε2/3	75	F	[41]

Abbreviations: FAD—Familial Alzheimer’s disease; HC—Healthy control; IC—Isogenic control; iPSC—induced pluripotent stem cell.

2.2. Neuronal Differentiation

To generate excitatory cortical neurons from induced pluripotent stem cells, a well-characterised protocol combines the use of a lentiviral vector to express the neurogenin-2 (NGN2) transcription factor and drive neuronal differentiation, as well as small molecules inhibiting TGF-β and BMP signalling (SB431542 and LDN193189) to drive neurons towards a forebrain identity [42]. Representative images of the cells and the differentiation timeline are shown in Supplementary Figure S1.

Differentiation of iPSCs to excitatory cortical neurons was performed according to Nehme et al. (2018) [42] with minor modifications. Throughout differentiation, cells were maintained in a humidified incubator at 37 °C with 5% CO₂ and 3% O₂. After being thawed from frozen stocks, iPSCs were passaged at least once before being differentiated into neurons. Once iPSCs achieved the desired confluence, they were dissociated to single cells with Accutase (Thermo Fischer Scientific) and counted with a Countess II Automated Cell Counter (Thermo Fischer Scientific) using Trypan Blue (Sigma-Aldrich; Burlington, MA, USA). Single cells were plated at the desired density depending on the assay with mTeSR1 (Stem Cell Technologies) and 10 μM Y-27632 (Focus Bioscience, St Lucia, QLD, Australia) in Matrigel (Corning) and Poly-D-lysine (10–50 μg/mL; Sigma-Aldrich) coated plates. After 24 h, the cells were transduced with lentivirus (1–2 μL virus/1 mL medium) containing rtTA

and NGN2-GFP expression vectors. The following day (day 0), the medium was replaced with neuronal differentiation medium containing 1 µg/mL doxycycline (Sigma-Aldrich), 10 µM SB431542 (Focus Bioscience), and 0.1 µM LDN-193189 (Focus Bioscience). On day 1, the culture medium was fully changed to a neuronal differentiation medium containing 1 µg/mL doxycycline, 10 µM SB431542, 0.1 µM LDN-193189, and 0.5 µg/mL puromycin. The same procedure was repeated on days 2 and 3. On day 4, the medium was gradually transitioned to neuronal maturation medium by adding 25% neuronal maturation medium and 75% neuronal differentiation medium containing 10 ng/mL BDNF (Miltenyi Biotec; Gladbach, Germany). The medium was changed every day until neurons were in 100% neuronal maturation medium (day 7). After that, a half-medium change was carried out every other day with neuronal maturation medium containing 1 µg/mL doxycycline and 10 ng/mL BDNF. Doxycycline was maintained until day 10 of differentiation. Neurons were grown until day 35 before experiments were conducted.

2.3. Lentivirus Production

Lentiviruses were produced by co-transfecting HEK293T cells (ATCC; Manassas, VA, USA) with two packaging plasmids, one envelope plasmid, and one transfer plasmid (NGN2 or rtTA). Throughout the experiment, the cells were maintained in a humidified incubator at 37 °C with 5% CO₂ and 3% O₂. For each lentivirus produced (NGN2 and rtTA), one T-75 flask was plated with 4 × 10⁶ HEK293T cells in DMEM/F12 with 1 × Glutamax (Thermo Fischer Scientific) and 5% fetal bovine serum (FBS; Gibco; Grand Island, NY, USA). The following day, 1.5 mL of Opti-MEM was mixed with the plasmid DNAs. On a different falcon tube, 75 µL of polyethylenimine (PEI) transfection reagent (3:1 ratio with DNA) was mixed with 1.5 mL of Opti-MEM (Gibco) and incubated for 5 min. Then, the DNA/Opti-MEM mix was combined with the PEI/Opti-MEM solution and incubated for 20 min to allow the formation of DNA/lipid complexes. This solution was then gently added to the T-75 flasks containing the HEK293T cells. After 5–7 h, the medium was discarded and replaced with fresh DMEM/F12 medium (with 1 × Glutamax and 5% FBS). The next day, the medium containing viral particles was collected and stored at 4 °C, and fresh medium was added to the cells. The same procedure was repeated for another two days. After 3 days of viral media collection, the media was combined and centrifuged at 200 × g for 2 min to pellet and remove HEK293T cells. The viral supernatant was filtered through a 50 mL syringe fitted with a 0.45 µm syringe filter and moved to an ultracentrifuge tube. The tubes were weighted to ensure they were within 0.1 g of each other, and, if necessary, sterile H₂O was added. The virus was spun at 23,500 rpm for 2 h at 4 °C in an ultracentrifuge. Following centrifugation, the supernatant was discarded and PBS (200 × initial volume) was added to the viral pellet, which was gently triturated for approximately 10 min. The viral particles were aliquoted and stored at –80 °C until further use.

2.4. Neuronal Characterization by Immunocytochemistry

Cells grown for immunocytochemistry were plated on glass coverslips coated with Matrigel (Corning) or Matrigel and Poly-D-lysine (10–50 µg/mL; Sigma-Aldrich) for iP-SCs and neurons, respectively. Cells were washed with TBS and fixed with 4% (*w/v*) paraformaldehyde (PFA) in PBS for 20 min, and then washed 3 times with TBS. Cells were permeabilised in 0.3% Triton X-100 in TBS for 10 min at room temperature. Following permeabilisation, cells were blocked in 10% goat serum in TBS for 1 h at room temperature. Then, cells were incubated with primary antibodies (in 10% goat serum in TBS) at specified dilutions overnight at 4 °C. The next day, cells were washed three times in wash buffer (0.1% triton X-100 in TBS) and incubated at room temperature for 1 h with the secondary antibody (in 10% goat serum in TBS) at specified dilutions. After that, cells were washed 3 times in wash buffer and incubated with Hoechst 33342 (1:1000; Thermo Fischer Scientific) in TBS for 15 min at room temperature. Then, cells were washed in TBS, and coverslips were mounted on glass slides using ProLong Gold Antifade Mountant (Thermo Fischer Scientific). Cells were imaged on the Leica TCS SP8 confocal microscope (Leica

Microsystems) and analysed with the Leica Application Suite—Advanced Fluorescence (LAS-AF) 2.6.1–7314 software (Leica Microsystems, Wetzlar, Germany). For the no primary antibody control, no primary antibody was added, and both secondary antibodies were added using the same conditions used for MAP2 and GFAP.

Antibodies: Anti-GFAP Chicken, pAb 1:800 Sigma-Aldrich #ab5541; Anti-MAP2 Mouse, mAb 1:200 Sigma-Aldrich #MAB3418; Anti-Oct4 Mouse, mAb 1:1000 Stem Cell Technologies #01550; Anti-SSEA-4 Mouse, mAb 1:200 Abcam #ab16287; Goat anti-mouse IgG (H + L) Alexa Fluor 488 Goat 1:1000 Thermo Fischer Scientific # A-11001; Goat anti-mouse IgG (H + L) Alexa Fluor 555 Goat 1:1000 Thermo Fischer Scientific # A-21422; Goat anti-chicken IgY (H + L) Alexa Fluor 647 Goat 1:1000 Thermo Fischer Scientific # A-21449.

2.5. Amyloid- β Enzyme-Linked Immunosorbent Assay (ELISA)

A β 40 and A β 42 levels were measured using an enzyme-linked immunosorbent assay (ELISA) (Thermo Scientific). The conditioned medium from cultured neurons was collected with 1 \times cComplete protease inhibitor cocktail (Roche, Switzerland) and 1 \times PhosphoSTOP phosphatase inhibitor (Roche). Assays were performed following the manufacturer's instructions. Absorbance at 450 nm was measured on a SpectraMax Plus Microplate Reader (Molecular Devices; San Jose, CA, USA). Each sample was measured in triplicate, and the final protein concentration was determined using a standard curve generated using the A β peptide standard provided in the assay kit.

The A β 40 and A β 42 enzyme-linked immunosorbent assays (ELISA) (Thermo Fischer Scientific) were performed as per the manufacturer's instructions.

2.6. Western Blotting for Tau: Protein Extraction

Cells were washed twice with 1 \times TBS and incubated with RIPA buffer (50 mM Tris HCl pH 7.4, 1% Sodium deoxycholate, 150 mM NaCl, 1 mM EDTA, 1% Triton-X and 0.1% SDS in MilliQ) containing 1 \times cComplete protease inhibitor cocktail (Roche) and 1 \times PhosphoSTOP phosphatase inhibitor (Roche) for 20 min on ice. Cell lysate was vortexed for 10 sec and centrifuged at 10,000 \times g for 5 min. The supernatant was transferred into a new microcentrifuge tube and stored at -80 °C until use.

2.7. Detergent Compatible (DC) Protein Assay

The Detergent Compatible Protein Assay (Bio-Rad; Hercules, CA, USA) was used to measure total protein concentration according to the manufacturer's instructions. A total of 5 μ L of sample was mixed with 25 μ L of reagent A' (cell lysate) or A (tissue lysate) and 200 μ L of reagent B and incubated for 10 min on an orbital plate rocker (Labnet; Edison, NJ, USA). Each sample was measured in triplicate, and the final protein concentration was determined using a standard curve generated using Bovine Serum Albumin (BSA; Sigma-Aldrich) diluted in either RIPA buffer or lysis buffer. Absorbance was read at 750 nm using a SpectraMax Plus Microplate Reader (Molecular Devices).

2.8. Western Blotting

Cell pellets were diluted in RIPA buffer. Samples were mixed with Laemmli buffer (Bio-Rad) containing 5% (*v/v*) 2-mercaptoethanol (Sigma-Aldrich). Samples were denatured at 70 °C for 10 min before being loaded into a 4–20% Criterion TGX Stain-Free gel (Bio-Rad). The Precision Plus Protein Dual Colour (Bio-Rad) molecular weight marker was also loaded into the gel. Samples were run in duplicates, and a pooled sample was run on all gels to normalise for variations between gels. Following separation by electrophoresis at 160 V for 50 min in SDS buffer, proteins were transferred to an Immobilon-P PVDF membrane (Merck Millipore; Burlington, MA, USA) at 100 V for 60 min in ice-cold transfer buffer. Total membrane protein was imaged with ChemiDoc MP (Bio-Rad). The membrane was then washed 3 \times in Tris-Buffered Saline with 0.1% (*v/v*) Tween (TBST) and blocked in 5% (*w/v*) skim milk or 10% goat serum in TBST for 1 h at room temperature. Incubation with primary antibodies in blocking solution was carried out overnight at 4 °C, and then the membrane

was washed 3× for 5 min in TBST before being incubated with secondary antibodies in blocking solution for 1 h at room temperature. Following this step, the membrane was washed 3× for 5 min in TBST and then incubated for 5 min with SuperSignal™ West Pico PLUS Chemiluminescent Substrate (Thermo Scientific). Protein bands were detected by chemiluminescence with Amersham 600 RGB (GE Healthcare; Chicago, IL, USA), and relative densitometry values were quantified using ImageLab (Bio-Rad). Each protein band was normalised to its respective total protein and the mean pool total protein.

Antibodies: Anti-AMPA1 Rabbit pAb 1:1000 Abcam #ab31232; Anti-AMPA2 Rabbit mAb 1:2000 Abcam #ab133477; Anti-AMPA3 Mouse mAb Merck Millipore #MAB5416; Anti-AMPA4 Rabbit mAb Cell Signalling #8070; Anti-Tau-5 Mouse mAb Abcam #ab80579; Anti-Tau s404 Rabbit mAb 1:2500 Abcam #ab92676; Abbreviations: mAb—monoclonal antibody; pAb—polyclonal antibody; Goat anti-mouse IgG (H + L) HRP Goat 1:5000 Merck Millipore #AP308P; Goat anti-rabbit IgG (H + L) HRP Goat 1:5000 Merck Millipore #AP307P.

2.9. Flexstation to Measure Calcium Responses to Glutamate, NMDA, AMPA and Kainate

To study neuronal calcium response, iPSC-derived neurons were grown in a clear bottom 96 Well Black Polystyrene Microplate (Corning) for 35 days. A minimum of 6 wells per cell line were used for each drug treatment (glutamate, NMDA, AMPA, and kainate). A standard bathing solution (SBS; 160 mM NaCl, 2.5 mM KCl, 5 mM CaCl₂, 1 mM MgCl₂, 5 mM glucose, and 10 mM HEPES) was used for baseline perfusion of neurons. A 60 mM high potassium (High K⁺, 102.5 mM NaCl, 2.5 mM KCl, 5 mM CaCl₂, 1 mM MgCl₂, 5 mM glucose, and 10 mM HEPES) buffer was used as a positive control due to its ability to depolarise neurons and induce a calcium response. To measure neuronal response to iGluR agonists, 100 μM glutamate (Tocris, UK), 100 μM NMDA (Tocris), 100 μM AMPA (Tocris), and 100 μM kainate (Tocris) were prepared in SBS. All buffers and drugs were made on the same day the assay was run and adjusted to have a pH of 7.4 and osmolarity between 310 and 320 mOsm, the same as the conditioned neuronal cultured media.

Neurons were washed with SBS and loaded with 2 μM Fura-2-AM buffer (Thermo Fischer Scientific) and Pluronic F-127 acid (20% *w/v* in DMSO; Biotium; Fremont, CA, USA) at 37 °C for 30 min. After incubation, cells were washed again in SBS for 30 min before recording was conducted at 37 °C using a FlexStation 3 Multi-Mode Microplate Reader (Molecular Devices). The fluorescence signal was measured per well, corresponding to the calcium response of the neuronal population grown on each well. Fura-2 fluorescence emission at 510 nm was recorded every four seconds following excitation at 340 and 380 nm. To each well, a total of three solutions (SBS, drug of interest, and High K⁺) were added, and fluorescence was measured. Baseline recordings in SBS were taken for 20 s before the addition of the first compound. Each compound was recorded for 60 s before the addition of the following compound. The drugs glutamate, NMDA, AMPA, or kainate were added after SBS, followed by 60 mM High K⁺. The maximum Ca²⁺ response was calculated from the maximum peak of the Fura-2 AM 340/380 nm excitation ratio normalised to baseline fluorescence ($\Delta F_{340/380}$). Wells that did not respond to high K⁺ were excluded from the analysis. The SoftMax Pro 7 software (Molecular Devices) was used for data acquisition.

2.10. RT-qPCR for AMPAR Subunits: RNA Extraction and Purification

After being washed twice in PBS, cells were harvested in TRIsure (Bioline; Cincinnati, OH, USA) and left to incubate for 5 min at room temperature. To each 1 mL of cells in TRIsure, 200 μL of chloroform was added, and the sample was shaken vigorously for 15 s and incubated for 15 min at room temperature. Then, cells were centrifuged at 12,000× *g* for 15 min at 4 °C. The upper aqueous phase (RNA) was transferred to a fresh tube, and 500 μL of isopropanol was added. The samples were incubated for 10 min at room temperature and then centrifuged at 12,000× *g* for 10 min at 4 °C. The supernatant was discarded, and the RNA pellet was washed with 70% ethanol and centrifuged at 7500× *g* for 5 min at 4 °C. The supernatant was removed, and the RNA pellet was air-dried for approximately 30 min. Once dried, the pellet was resuspended in UltraPure DNase/RNase-Free Distilled Water

(Thermo Fischer Scientific). The NanoDrop 2000c (Thermo Fischer Scientific) was used to measure nucleic acid concentration and purity.

To remove genomic DNA, the TURBO DNA-free kit (Thermo Fischer Scientific) was used following the manufacturer's instructions. The RNA was diluted in 50 μ L of nuclease-free water, and 1 \times TURBO DNase buffer and 1 μ L TURBO DNase inactivation reagents were added. After the solution was incubated at 37 $^{\circ}$ C for 30 min, the DNase Inactivation Reagent was added and incubated for 5 min at room temperature. The samples were centrifuged at 10,000 \times g for 90 s, and the supernatant (RNA) was transferred to a fresh tube. RNA concentration was calculated with NanoDrop 2000c. The treated RNA was purified by ethanol precipitation. The RNA was diluted in 200 μ L UltraPure DNase/RNase-Free Distilled Water and mixed with 220 μ L isopropanol and 20 μ L 3 M sodium acetate. After being vortexed, the samples were kept at -80° C overnight and then centrifuged at 16,000 \times g for 20 min at 4 $^{\circ}$ C. The supernatant was removed, and the pellets were washed with 70% ethanol before being centrifuged at 16,000 \times g $^{\circ}$ C for another 2 min. The supernatant was discarded, and the pellet was air dried for approximately 30 min before being resuspended in UltraPure DNase/RNase-Free Distilled Water. The final concentration and purity of mRNA were measured using NanoDrop 2000c.

2.11. cDNA Synthesis

Complementary DNA (cDNA) was synthesised using the Tetro cDNA Synthesis Kit (Bioline). The protocol was followed according to the manufacturer's instructions: 2 μ g RNA was mixed with 1 μ L oligo (dT)18, 1 μ L 10 mM dNTP mix, 1 μ L tetro reverse transcriptase enzyme, 4 μ L 5 \times RT buffer, 1 μ L RNase inhibitor, and enough RNase-free water to complete the 20 μ L solution. Samples were incubated for 30 min at 45 $^{\circ}$ C, followed by 5 min at 85 $^{\circ}$ C, in the Mastercycler Pro (Eppendorf, Germany).

2.12. qPCR

Primers designed for the coding regions of the genes of interest and primers for housekeeper genes B2M, GAPDH, and HPRT1 were used (Table 2). Each cDNA sample was run in triplicate using 30 ng of cDNA per reaction. No reverse transcriptase RNA control and no template control were run as negative controls. QuantStudio 5 (Thermo Fischer Scientific) was used with the following settings: denaturation at 95 $^{\circ}$ C for 2 min, followed by 40 cycles of denaturation at 95 $^{\circ}$ C for 10 s, annealing at a specific primer melting temperature for 10 s, and extension at 72 $^{\circ}$ C for 10 s. The melt curve protocol started at 95 $^{\circ}$ C for 5 s, followed by 65 $^{\circ}$ C for 1 min, ramping up to 97 $^{\circ}$ C. Primers are listed in Table 2.

Table 2. List of primers used for reverse transcription-quantitative polymerase chain reaction (RT-qPCR).

Target	Sequence	Tm
B2M	F: AAGGACTGGTCTTTCTATCTC R: GATCCCACTTAACTATCTTGG	55 $^{\circ}$ C
GAPDH	F: GAGCACAAGAGGAAGAGAGACCC R: GTTGAGCACAGGGTACTTTATTGATGGTACATG	58 $^{\circ}$ C
HPRT1	F: TGACACTGGCAAAACAATGCA R: GGTCTTTTCACCAGCAAGCT	58 $^{\circ}$ C
GRIA1	F: CTAGAAGATCCTTATGTGATGC R: CTCCGTATTTCCATCACTG	58 $^{\circ}$ C
GRIA2	F: GGAATCTCCGTATGTTATGATG R: TTGACTTGAACCCACAATG	55 $^{\circ}$ C
GRIA3	F: TATTGTATCTGGGGCGTTAC R: TTGAGAACTCAAGAAGGGAG	55 $^{\circ}$ C
GRIA4	F: GGTACGATAAAGGTGAATGTG R: AAAAGGTCAGCTTCATTCTC	58 $^{\circ}$ C

Abbreviations: F—forward; R—reverse; Tm—primer melting temperature.

2.13. Data Analysis

Data analysis was performed in R v3.3.1 (<https://www.r-project.org>, accessed on 16 March 2023) using packages 'library(readxl)', 'library(ggplot2)', 'library(ggpubr)', 'library(lme4)', and 'library(lmerTest)'. The normal distribution of the data was assessed with a Shapiro–Wilk test using the function 'shapiro.test()'. Data not normally distributed were normalised via logarithmic (log2 or log10), square root (sqrt), or reciprocal (1/x) transformation. For comparison between disease and control groups, the data were subjected to linear regression modelling using the 'lm()' function, with independent differentiations included as co-variates.

3. Results

3.1. Generation of iPSC-Derived Neurons from FAD and Control Lines

Our aim in this study was to specifically assess the early calcium phenotypes of AD, and for this reason, we used day 35 of neuronal maturation, in which cells express neuronal markers and neuronal ion channels but may not yet demonstrate AD pathology. In this well-characterised protocol to generate excitatory cortical neurons, Nehme et al. (2018) [42] demonstrated by RNAseq the expression of AMPAR subunits GluA1-4 over time and found no expression of genes for hindbrain, inhibitory, hypothalamic, diencephalic, hippocampal, dopaminergic, and spinal motor neurons. Single-cell RT-qPCR of day 21 neurons detected mainly markers of cortical upper layer neurons, which was also confirmed by immunostaining and no expression of inhibitory neurons or glia. Furthermore, patch clamping experiments after 28 days of differentiation demonstrated that approximately 75% of the cells recorded were able to fire multiple action potentials [42]. Application of the AMPAR and NMDAR antagonists, NBQX and D-AP5, respectively, showed each compound individually reduced spiking rates and the occurrence of network-wide bursts, confirming the functional expression of AMPAR and NMDARs [42]. On the other hand, the GABA_A receptor antagonist, picrotoxin, caused no changes in firing rates or the occurrence of network-wide bursts [42].

To study AD phenotypes in a 2D cell culture model using iPSC-derived neurons, a total of 6 iPSC lines were used, including two familial Alzheimer's disease cell lines (FAD1 and FAD2) and their respective isogenic controls (IC1 and IC2) and two healthy controls (HC1 and HC2) (Table 1). Each FAD line contains a different mutation in the *PSEN1* gene, which causes early-onset familial Alzheimer's disease, while the isogenic controls have the same genome as their respective FAD lines, with the exception of the FAD mutation, which has been reverted back to WT. HC1 cells were obtained from a healthy donor with no known family association with FAD1, while the HC2 cell line donor is a healthy family relative of FAD2. Due to their genetic background and family associations, throughout this study, FAD1 neurons were compared against their isogenic control (IC1) and HC1 only, while FAD2 neurons were compared against IC2 and HC2.

To generate iPSC-derived neurons from AD patients, isogenic controls, and healthy individuals, a previously published protocol using small molecules and NGN2 lentivirus was used to generate cortical excitatory neurons [42]. The neurons were differentiated for a total of 35 days prior to analysis.

iPSC-Derived Neurons Express Neuronal Marker MAP2

To confirm the generation of iPSC-derived neurons after 35 days of differentiation, immunocytochemistry was used. Immunostaining against microtubule-associated protein 2 (MAP2), a neuron-specific cytoskeletal protein, confirmed extensive expression of this marker in all 6 cell lines (FAD1, IC1, HC1, FAD2, IC2, and HC2) (Figures 1 and 2). To check for the presence of glial cells, the cells were also stained against the glial fibrillary acidic protein (GFAP), a type III intermediate filament protein expressed in glial cells. However, no positive staining was observed for GFAP for any of the 6 cell lines (Figures 1 and 2). A non-primary antibody control showed no signal for the MAP2 and GFAP channels

(Supplementary Figures S2 and S3). These results confirm the generation of neurons and the absence of GFAP-positive cells after 35 days of differentiation.

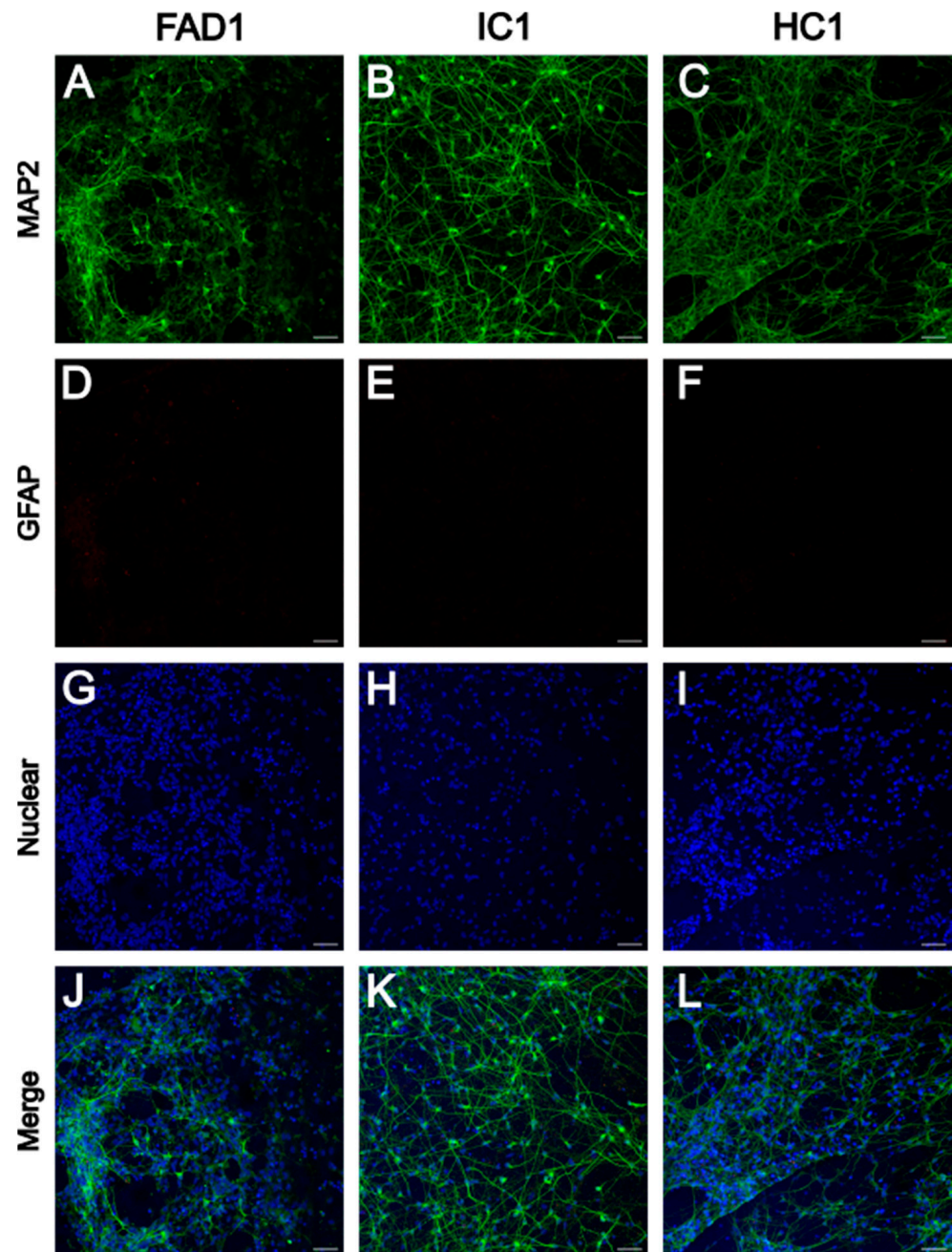


Figure 1. MAP2 and GFAP immunoreactivity in FAD1, IC1, and HC1 iPSC-derived neurons. Representative images showing MAP2 (A–C), GFAP (D–F), the nuclear marker Hoechst (G–I), and the merged image (J–L) from FAD1, IC1, and HC1. Scale bar = 50 μ m. FAD—familial Alzheimer’s disease; HC—healthy control; IC—isogenic control.

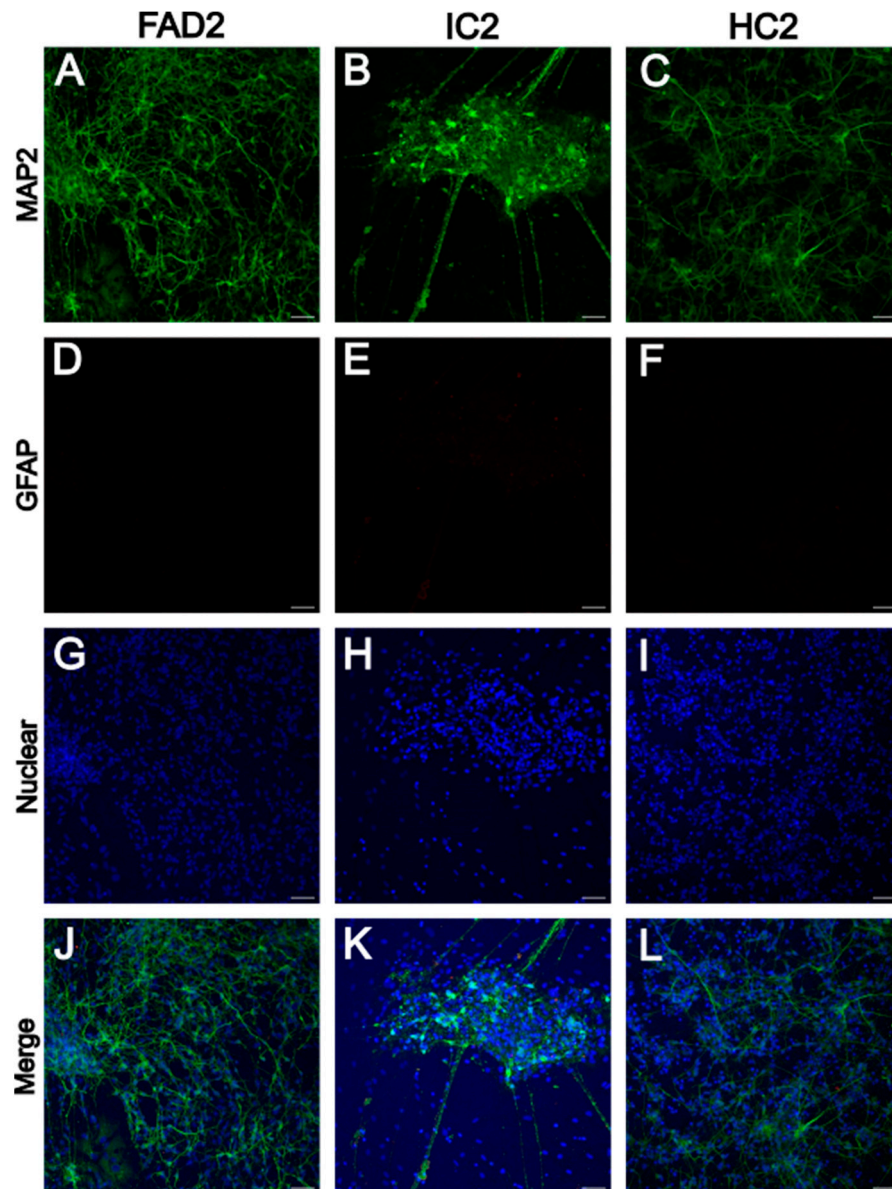


Figure 2. MAP2 and GFAP immunoreactivity in FAD2, IC2, and HC2 iPSC-derived neurons. Representative images showing MAP2 (A–C), GFAP (D–F), the nuclear marker Hoechst (G–I), and the merged image (J–L) from FAD2, IC2, and HC2. Scale bar = 50 μ m. FAD—familial Alzheimer’s disease; HC—healthy control; IC—isogenic control.

3.2. FAD NGN2-Derived iPSC Neurons Did Not Show Evidence of A β Pathology at Day 35 of Maturation

The decreased A β 42/A β 40 ratio in both CSF and plasma is an important biomarker of AD [43,44]. While A β 40 is the most abundant A β peptide, A β 42 is more prone to aggregation. Due to inter-individual differences in A β peptide production, the A β 42/A β 40 ratio is considered a more accurate measurement of A β pathology than the levels of A β 42 alone [43,45,46].

In 2D in vitro cultures, since A β plaques cannot be formed due to the regular medium changes, the elevated production of A β 42 results in a higher A β 42/A β 40 ratio in some long-term cell culture models [36,47–50]. For example, in day >50–60 neurons, both A β and tau pathology can be identified in AD neurons [47,48]. To measure the A β 42/A β 40 ratio in disease and control day 35 neurons in this study, an ELISA was performed using medium from neuronal cultures collected at day 35 of differentiation to quantify both A β 40 and A β 42 levels separately.

While no significant differences were detected in A β 40 concentration between disease (FAD1— 152.1 ± 38.64 , FAD2— 223.7 ± 51.23) and isogenic control (IC1— 150.1 ± 45.28 , $p = 0.642$; IC2— 249.6 ± 68.31 , $p = 0.846$) or healthy control (HC1— 206 ± 77.18 , $p = 0.143$; HC2— 187.8 ± 52.06 , $p = 0.122$) cell lines (Figure 3A), FAD2 (9.37 ± 1.859) neurons showed significantly higher levels of A β 42 compared to HC2 (5.346 ± 0.994 ; $p = 0.001$), but no significant differences compared to IC2 (8.333 ± 1.168 ; $p = 0.448$) (Figure 3B). For the cell lines FAD1, IC1, and HC1, the concentration of A β 42 in the medium could not be quantified as it was below the detection threshold of the assay, and therefore the A β 42/A β 40 ratio could not be calculated. No significant differences were found between the FAD2 (0.044 ± 0.005) and control cell lines (HC2— 0.032 ± 0.005 , $p = 0.281$; IC2— 0.041 ± 0.01 , $p = 0.782$) in the A β 42/A β 40 ratio (Figure 3C).

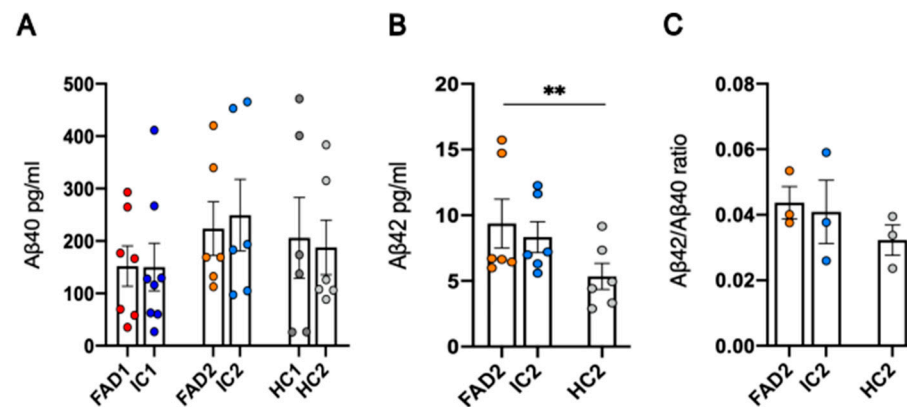


Figure 3. A β 42/A β 40 ratio in neuronal cultures. A β 40 (A) and A β 42 (B) levels were measured separately in pg/mL by ELISA and were used for calculation of the A β 42/A β 40 ratio (C). Data shown are day 35 neurons, $n = 2$ replicates from 3–4 independent differentiations, and error bars represent \pm SEM. For the A β 42/A β 40 ratio, data = mean \pm SEM, ** $p < 0.01$. Data are normally distributed (FAD2/HC2/IC2 A β 42/A β 40 ratio) or normalised to \log_2 (FAD1/HC1/IC1 A β 40), $\sqrt{\text{FAD2/HC2/IC2 A}\beta 42}$, or $1/x$ (FAD2/HC2/IC2 A β 40) and analysed by linear regression modelling. Independent differentiations were included as co-variates. FAD—familial Alzheimer’s disease; HC—healthy control; IC—isogenic control.

These results indicate A β 40 levels can be detected in the conditioned medium of iPSC-derived neurons, but the levels of A β 42 may be too low to allow detection by commercial assays. For the group of cell lines in which both A β 42 and A β 40 could be measured, FAD1 iPSC-derived day 35 neurons did not show AD-associated changes in A β 42/A β 40 ratios.

3.3. FAD NGN2 Derived iPSC Neurons Did Not Show Tau Pathology at Day 35 of Maturation

Intracellular accumulation of misfolded phosphorylated tau (p-Tau) protein is a molecular hallmark of AD that is associated with cognitive decline. Our previous work has shown that day >50–60 AD neurons demonstrate increased phosphorylated tau relative to total tau, consistent with AD-related tau pathology [48]. To assess whether day 35 neurons demonstrate tau phenotypes, we performed western blotting to measure total tau (Tau-5) and phosphorylated tau at serine 404 (p-Tau S404) protein levels between AD and control neurons after 35 days of differentiation (Figure 4A,B). Although tau phosphorylation occurs at different protein epitopes, phosphorylation at serine 404 is one of the earliest events in tau pathology [51], hence why p-Tau S404 was chosen as a marker of AD pathology for this neuronal model of AD. For both Tau-5 and p-Tau S404 western blots, a single band of approximately 50 kDa was observed.

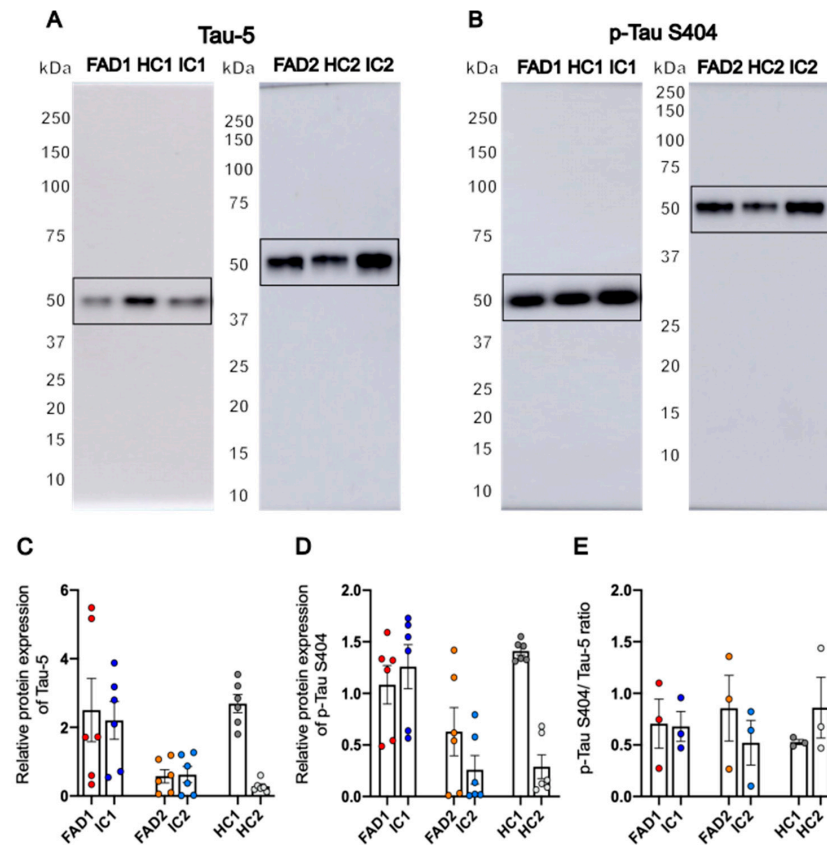


Figure 4. Expression of phosphorylated and total protein tau in neuronal cultures. Representative western blots of Tau-5 (A) and p-Tau S404 (B) and relative protein expression of Tau-5 (C) and p-Tau S404 (D) and ratio of p-Tau S404/Tau-5 relative protein expression (E). Data shown are day 35 neurons; $n = 2$ replicates from 3 independent differentiations, normalised to total protein; error bars represent \pm SEM. For the p-Tau S404/Tau-5 ratio, data = mean \pm SEM. Data are normally distributed (FAD1/HC1/IC1 and FAD2/HC2/IC2 p-Tau S404/Tau-5 ratio and FAD1/HC1/IC1 Tau-5 and p-Tau S404) or normalised to \log_{10} (FAD2/HC2/IC2 p-Tau S404) or $\sqrt{\text{FAD2/HC2/IC2 Tau-5}}$ and analysed by linear regression modelling. Independent differentiations were included as co-variables; there were no significant differences between groups. FAD—familial Alzheimer’s disease; HC—healthy control; IC—isogenic control; p-Tau—phosphorylated tau.

Regarding protein expression of Tau-5, there were no significant differences between FAD (FAD1— 2.505 ± 0.923 , FAD2— 0.575 ± 0.194) and control cell lines (HC1— 2.69 ± 0.265 , $p = 0.84$; IC1— 2.202 ± 0.551 , $p = 0.742$; HC2— 0.283 ± 0.069 , $p = 0.299$; IC2— 0.624 ± 0.231 , $p = 0.919$) (Figure 4C and Supplementary Figures S4 and S5). Similar results were obtained after analysis of the relative protein amount of p-Tau S404. FAD neurons (FAD1— 1.084 ± 0.187 , FAD2— 0.629 ± 0.234) showed no significant differences compared to their isogenic or healthy controls (HC1— 1.41 ± 0.04 , $p = 0.073$; IC1— 1.259 ± 0.213 , $p = 0.316$; HC2— 0.29 ± 0.115 , $p = 0.819$; IC2— 0.259 ± 0.139 , $p = 0.274$) (Figure 4D and Supplementary Figures S6 and S7). The ratio of phosphorylated S404 Tau to Tau-5 (total tau) normalised to total protein was calculated to compensate for variations in the production and clearance of tau between cell lines. Data analysis using linear regression modelling showed there were no significant differences between the FAD lines (FAD1— 0.706 ± 0.239 , FAD2— 0.856 ± 0.319) and their respective isogenic (IC1— 0.679 ± 0.145 , $p = 0.91$; IC2— 0.521 ± 0.217 , $p = 0.43$) and healthy controls (HC1— 0.527 ± 0.024 , $p = 0.465$; HC2— 0.861 ± 0.294 , $p = 0.99$) (Figure 4E).

Overall, both Tau-5 and p-Tau S404 proteins were detected in all cell lines, with no significant differences between FAD and control neurons. These results show that iPSC-derived neurons from FAD donors at day 35 of differentiation did not show the AD-associated phenotype of abnormally elevated S404 tau phosphorylation.

3.4. FAD Neurons Demonstrated Increased AMPAR Ca^{2+} Signalling Compared to Isogenic Controls

Dysfunctional calcium signalling and abnormal glutamatergic transmission are common phenotypes of AD. To assess if these phenotypes were recapitulated in iPSC-derived FAD neurons even in the absence of $A\beta$ and tau phenotypes, quantification of calcium responses was conducted in Alzheimer's disease, isogenic control, and healthy control day 35 neurons. Neurons were treated with 60 mM High K^+ (to mimic depolarisation), and Ca^{2+} responses were quantified. Ca^{2+} responses were also quantified following the application of 100 μ M glutamate, NMDA, AMPA, or kainate in iPSC-derived neurons from FAD patients and controls. Live cell calcium imaging was performed by loading the cells with the ratiometric dye Fura-2 AM prior to treatments. The Flexstation microplate reader was used to measure Ca^{2+} signals from a population of neurons in the wells of a 96 well plate. The maximum Ca^{2+} response from each well was calculated from the maximum peak of the Fura-2 AM 340/380 nm excitation ratio normalised to baseline fluorescence ($\Delta F_{340/380}$).

3.5. The iPSC-Derived Neurons Displayed Ca^{2+} Responses to High K^+

To verify if day 35 neurons were able to depolarise and produce Ca^{2+} responses, the cells were treated with a high concentration of K^+ (High K^+ , 60 mM). After loading the neurons with Fura-2 AM, a standard bathing solution (SBS) was added to the cells to allow the measurement of baseline fluorescence, then High K^+ was applied and Ca^{2+} signals were quantified. Neurons from all cell lines exhibited an increase in the 340/380 fluorescence ratio, indicative of Ca^{2+} responses (Figure 5A,B).

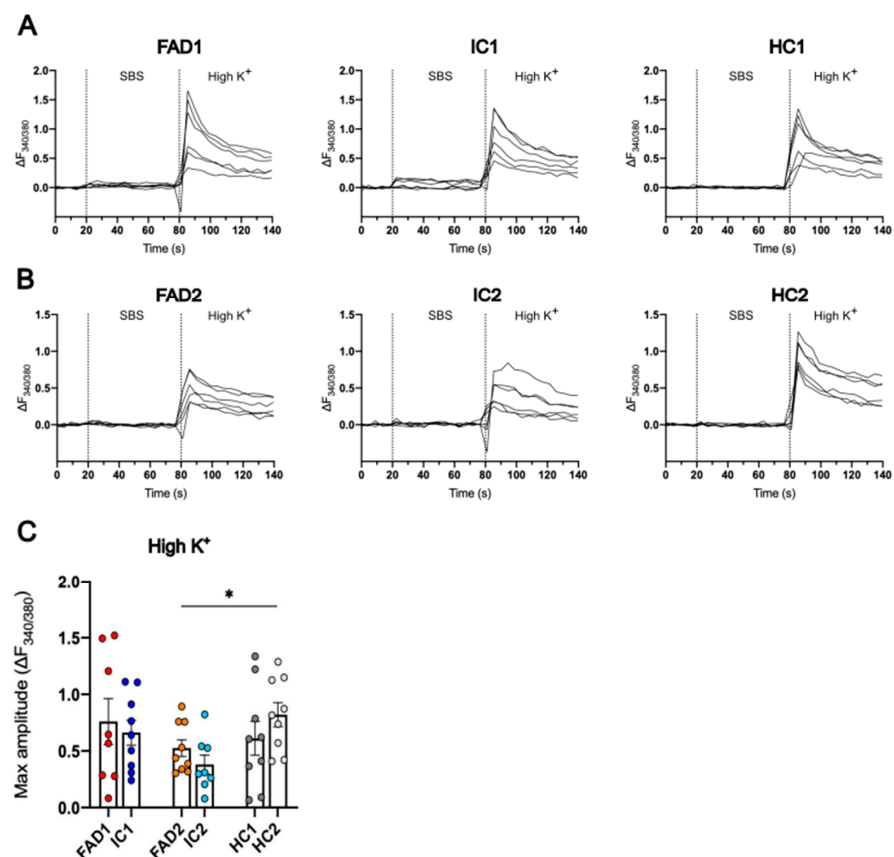


Figure 5. High K^+ elicits Ca^{2+} responses in iPSC-derived neurons. Representative traces of the change in fluorescence signal ratio over baseline ($\Delta F_{340/380}$) in response to 60 mM K^+ (High K^+) were recorded from FAD1/IC1/HC1 (A) and FAD2/IC2/HC2 neurons (B). The maximum Ca^{2+} response to High K^+ was calculated as the maximum amplitude of the Fura-2 AM fluorescence ratio change over baseline ($\Delta F_{340/380}$) (C). Day 35 neurons were loaded with the ratiometric dye Fura-2 AM, perfused with SBS, and treated with High K^+ . Data shown are single wells of a 96-well plate containing day 35 neurons,

n = 8–15 replicates from three independent differentiations; error bars represent \pm SEM; * $p < 0.05$ (FAD2 vs. HC2, but not IC2). Data are normally distributed and analysed using linear regression modelling. Independent differentiations were included as co-variables. FAD—familial Alzheimer’s disease; HC—healthy control; IC—isogenic control.

FAD2 neurons (0.525 ± 0.074) had a significantly lower Ca^{2+} response than HC2 cells (0.821 ± 0.107 , $p = 0.026$), which displayed the highest maximum amplitude of all cell lines. Although IC2 (0.38 ± 0.083 , $p = 0.272$) neurons had the lowest maximum amplitude, this value was not significantly different from the FAD2 line. The peak $\Delta\text{F}_{340/380}$ of FAD1 (0.760 ± 0.202) cells had no statistically significant difference from IC1 (0.662 ± 0.111 , $p = 0.442$) and HC1 (0.612 ± 0.149 , $p = 0.249$) cells (Figure 5C).

In sum, iPSC-derived day 35 neurons depolarised and displayed Ca^{2+} signals after treatment with 60 mM K^+ . There were no significant differences in these responses between the FAD and IC neurons.

3.6. FAD Neurons Displayed Increased Ca^{2+} Responses to Glutamate

Glutamate, as the main excitatory neurotransmitter in the CNS, is an important regulator of synaptic plasticity in the brain. However, numerous studies have reported aberrant neuronal excitability in AD patients and lab models of the disease [32]. To investigate how day 35 iPSC-derived neurons respond to glutamatergic stimuli, neurons were treated with 100 μM glutamate, and the Fura-2 AM 340/380 nm excitation ratio normalised to baseline fluorescence ($\Delta\text{F}_{340/380}$) was recorded over time.

Neurons from all FAD, IC, and HC cell lines displayed Ca^{2+} responses to glutamate (Figure 6A,B). To compare the maximum amplitude of Ca^{2+} responses to glutamate between cell lines, the maximum peak of the Fura-2 AM 340/380 nm fluorescence change ($\Delta\text{F}_{340/380}$) over baseline was calculated. This analysis confirmed that FAD1 (0.686 ± 0.111) neurons showed significantly higher Ca^{2+} responses compared to IC1 (0.446 ± 0.056 , $p = 0.033$) and HC1 (0.377 ± 0.047 , $p = 0.005$). Similarly, FAD2 (0.530 ± 0.095) neurons had significantly greater Ca^{2+} responses to 100 μM glutamate than neurons from the relevant isogenic control IC2 (0.345 ± 0.067 , $p = 0.013$), but were not significantly different from neurons from the HC2 line (0.526 ± 0.040 , $p = 0.570$) (Figure 6C). Thus, FAD iPSC-derived day 35 neurons showed elevated Ca^{2+} signals in response to treatment with 100 μM glutamate compared to their relevant isogenic controls.

3.7. FAD Neurons Displayed Increased Ca^{2+} Responses to AMPA but Not NMDA or Kainate Compared to Their Isogenic Control Lines

Glutamate can act on two subgroups of receptors in the post-synapse: mGluRs and iGluRs. The latter are divided into AMPAR, NMDAR, and KAR, and their activation mediates fast excitatory synaptic transmission and modulates synaptic plasticity. To investigate the contribution of specific iGluRs in the elevated Ca^{2+} responses of FAD neurons to glutamate, day 35 iPSC-derived neurons were treated with the AMPAR, NMDAR, and KAR agonists: AMPA, NMDA, and kainate, respectively.

Tracking of the 340/380 fluorescence change ($\Delta\text{F}_{340/380}$) over time showed all 6 cell lines responded to 100 μM AMPA (Figure 7A,B). Statistical analysis of the maximum amplitude of $\Delta\text{F}_{340/380}$ showed both FAD1 (0.709 ± 0.088) and FAD2 (0.673 ± 0.125) exhibited higher Ca^{2+} responses to 100 μM AMPA than their respective isogenic controls, IC1 (0.289 ± 0.048 , $p = 1.53 \times 10^{-5}$) and IC2 (0.330 ± 0.086 , $p = 0.010$). FAD1 also had increased Ca^{2+} responses to 100 μM AMPA compared to HC1 (0.432 ± 0.075 , $p = 0.017$); however, FAD2 and HC2 (0.406 ± 0.067 , $p = 0.077$) were not significantly different (Figure 7C).

Treatment with 100 μM NMDA showed no significant differences in Ca^{2+} responses from FAD1 (0.380 ± 0.085) and FAD2 (0.41 ± 0.134) relative to their isogenic controls, IC1 (0.353 ± 0.064 , $p = 0.874$) and IC2 (0.337 ± 0.132 , $p = 0.692$), respectively. However, FAD1 (0.38 ± 0.085) Ca^{2+} signals were significantly elevated compared to HC1 (0.139 ± 0.014 , $p = 0.046$), while no significant differences were observed between FAD2 and HC2 (0.422 ± 0.1 , $p = 0.307$) (Figure 7D).

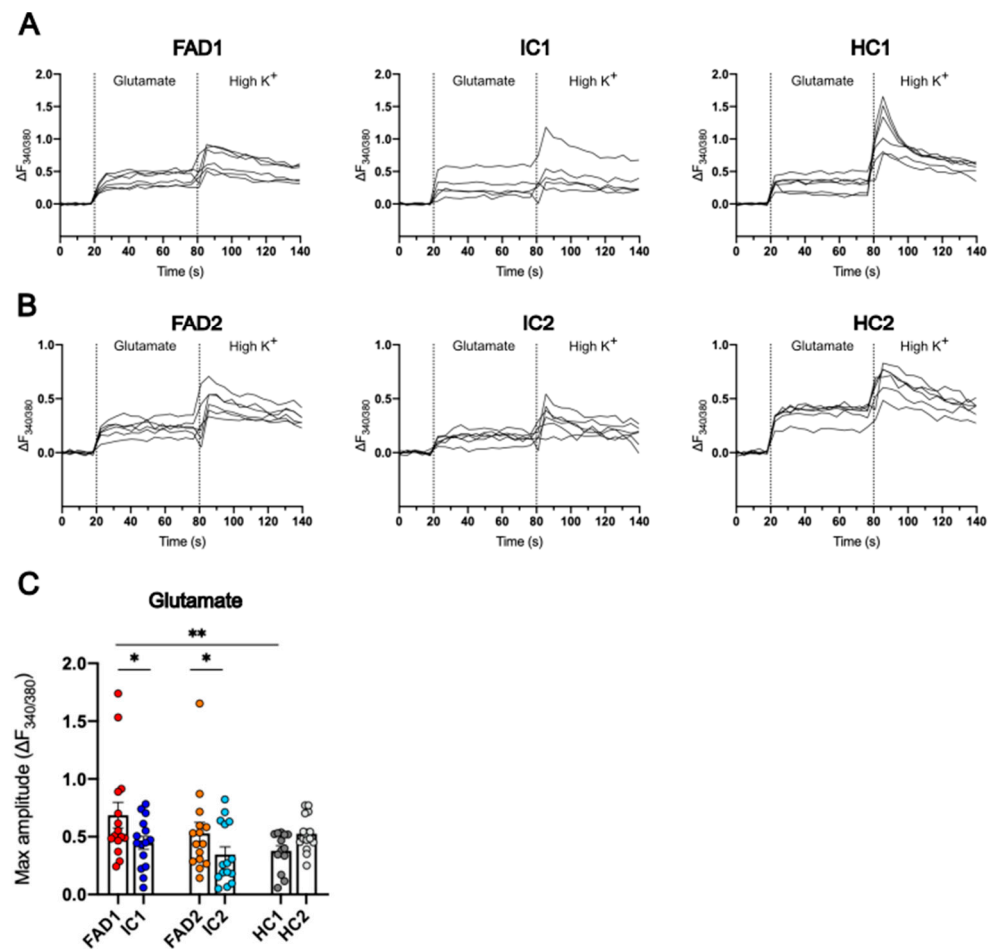


Figure 6. Ca^{2+} responses to glutamate are increased in FAD neurons. Representative traces of the change in fluorescence signal ratio over baseline ($\Delta F_{340/380}$) in response to 100 μM glutamate were recorded from FAD1/IC1/HC1 (A) and FAD2/IC2/HC2 neurons (B). The maximum Ca^{2+} response to 100 μM glutamate was calculated as the maximum amplitude of the Fura-2 AM fluorescence ratio change over baseline ($\Delta F_{340/380}$) (C). Day 35 neurons were loaded with the ratiometric dye Fura-2 AM, perfused with SBS, and treated with 100 μM glutamate, followed by 60 mM K^+ (High K^+). Data shown are single wells of a 96-well plate containing day 35 neurons; $n = 8$ –15 replicates from three independent differentiations; error bars represent \pm SEM; * $p < 0.05$, ** $p < 0.01$. Data were normalised to sqrt (FAD1/HC1/IC1) or log2 (FAD2/HC2/IC2) and analysed using linear regression modelling. Independent differentiations were included as co-variates. FAD—familial Alzheimer’s disease; HC—healthy control; IC—isogenic control.

Analysis of Ca^{2+} signals following 100 μM kainate treatment revealed no significant differences between the FAD (FAD1 = 0.636 ± 0.111 ; FAD2 = 0.37 ± 0.037) lines and their isogenic controls (IC1 = 0.39 ± 0.069 , $p = 0.128$; IC2 = 0.42 ± 0.051 , $p = 0.446$). Additionally, FAD1 and HC1 (0.47 ± 0.067 , $p = 0.604$) had no significant differences. Nonetheless, HC2 (0.601 ± 0.049 , $p = 0.001$) neurons had greater Ca^{2+} responses to 100 μM kainate compared to FAD2 (0.37 ± 0.037) (Figure 7E).

Taken together, these data confirm that day 35 iPSC-derived neurons respond to excitatory stimulus and that FAD neurons display abnormally elevated Ca^{2+} signals when treated with glutamate and, more specifically, the AMPAR agonist AMPA, but not with NMDA or kainate. This suggests FAD neurons demonstrate a glutamatergic Ca^{2+} signalling phenotype, contributed (at least in part) by increased AMPAR signalling.

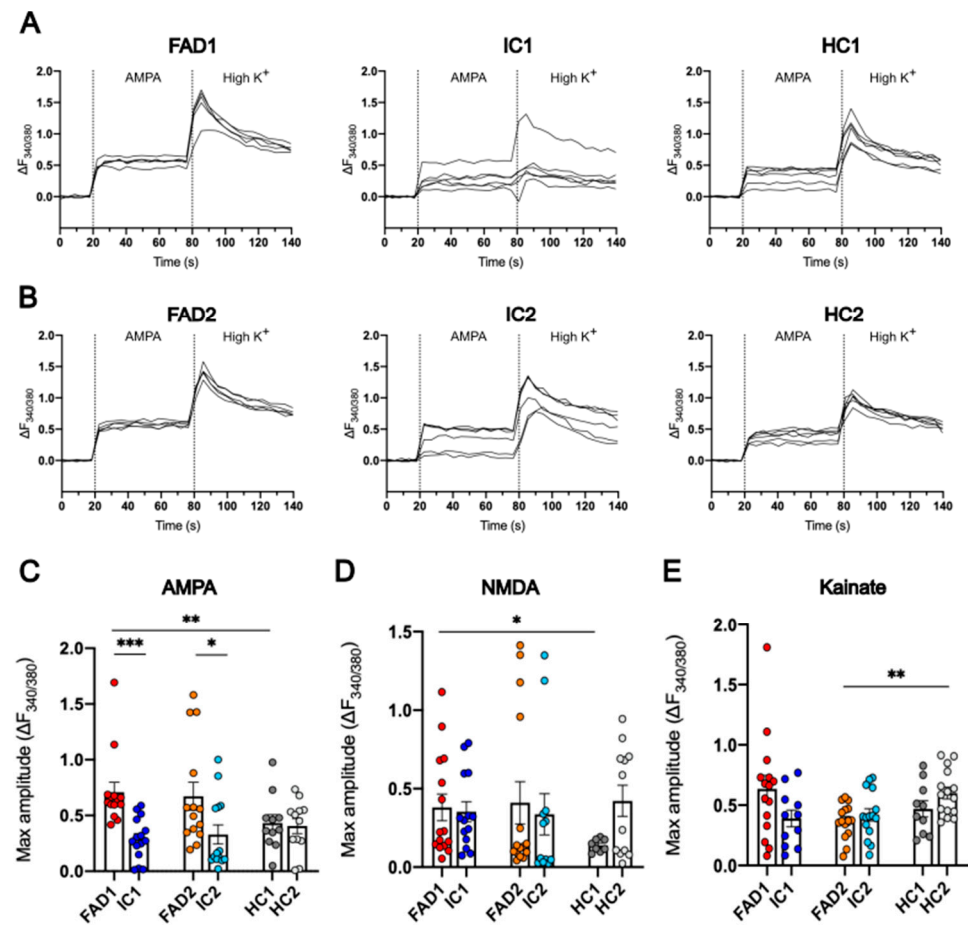


Figure 7. Ca^{2+} responses to AMPA are increased in FAD neurons. Representative traces of the change in fluorescence signal ratio over baseline ($\Delta F_{340/380}$) in response to 100 μM AMPA were recorded from FAD1/IC1/HC1 (A) and FAD2/IC2/HC2 neurons (B). The maximum Ca^{2+} response to 100 μM AMPA (C), 100 μM NMDA (D), and 100 μM kainate (E) was calculated as the maximum amplitude of the Fura-2 AM fluorescence ratio change over baseline ($\Delta F_{340/380}$) (C). Day 35 neurons were loaded with the ratiometric dye Fura-2 AM, perfused with SBS, and treated with either 100 μM AMPA, 100 μM NMDA, or 100 μM kainate, followed by 60 mM K^+ (High K^+). Individual data points are from individual wells of a 96-well plate containing day 35 neurons; $n = 8$ –15 replicates from three independent differentiations; error bars represent \pm SEM; *** $p < 0.001$ (AMPA: FAD1 vs. IC1); ** $p < 0.01$ (AMPA: FAD1 vs. HC1; Kainate: FAD2 vs. HC2); * $p < 0.05$ (AMPA: FAD2 vs. IC2; NMDA: FAD1 vs. HC1). Data are normally distributed (FAD2/HC2/IC2 kainate) or normalised to log2 (FAD1/HC1/IC1 kainate and NMDA and FAD2/HC2/IC2 NMDA) or sqrt (FAD1/HC1/IC1 and FAD2/HC2/IC2 AMPA) and analysed using linear regression modelling. Independent differentiations were included as co-variates. FAD—familial Alzheimer’s disease; HC—healthy control; IC—isogenic control.

3.8. Regulation at the Level of mRNA or Protein of the AMPA Receptor Subunits Does Not Explain the Increased Calcium Responses to AMPA in FAD Neurons Compared to Isogenic Control Neurons

Since the FAD neurons exhibited significantly increased maximum Ca^{2+} responses to AMPA, we next investigated whether changes in mRNA or protein levels of the AMPAR subunits may be responsible for the increased signalling. To test this hypothesis, RT-qPCR was performed to investigate if differences observed in neuronal Ca^{2+} responses to AMPA between FAD and isogenic control neurons were due to differences in mRNA expression of AMPAR subunits 1–4 encoded by the genes *GRIA1*, *GRIA2*, *GRIA3*, and *GRIA4* (Figure 8A–D).

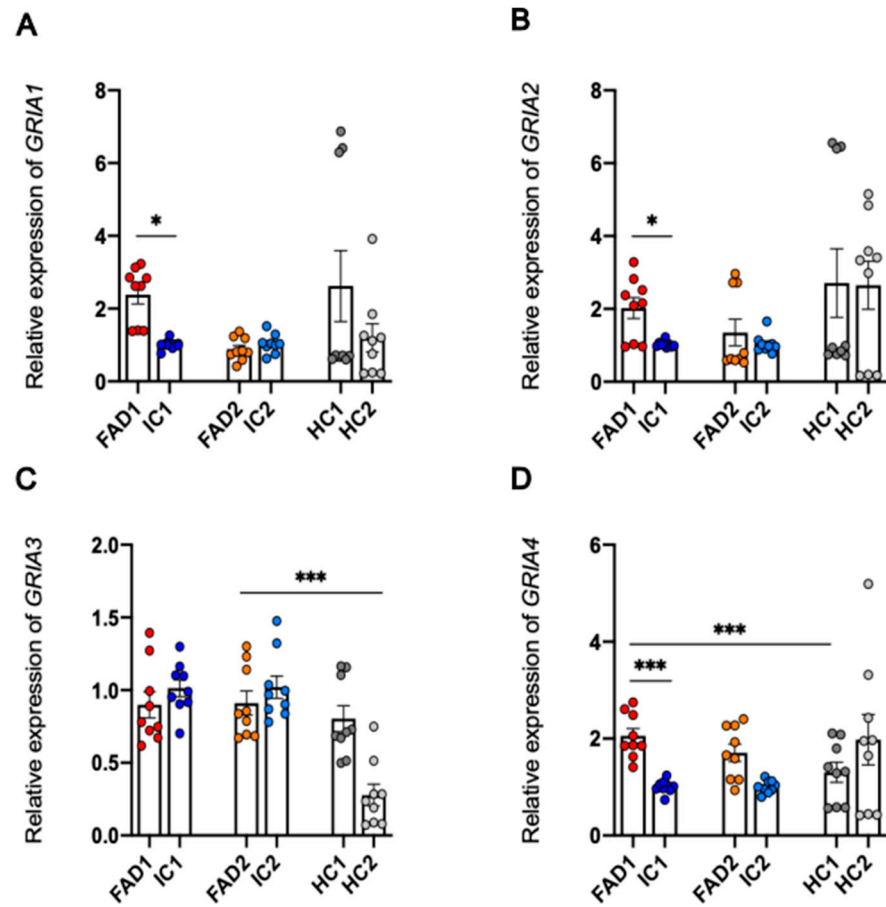


Figure 8. AMPAR subunits mRNA expression of FAD and control neurons. RT-qPCR analysis of GRIA1 (A), GRIA2 (B), GRIA3 (C), and GRIA4 (D) mRNA expression of day 35 neurons normalised to housekeeper genes GAPDH, HPRT1, and B2M. Data shown are replicates from one experiment using cDNA collected from three independent differentiations run in triplicate; error bars represent \pm SEM; * $p < 0.05$, *** $p < 0.001$. Data are normally distributed (FAD1/HC1/IC1 GRIA3 and GRIA4 and FAD2/HC2/IC2 GRIA3) or normalised to log₂ (FAD1/HC1/IC1 GRIA1 and FAD2/HC2/IC2 GRIA1, GRIA2 and GRIA4) or 1/x (FAD1/HC1/IC1 GRIA2) and analysed using linear regression modelling. Independent differentiations were included as co-variates. FAD—familial Alzheimer's disease; HC—healthy control; IC—isogenic control.

Expression of *GRIA1* mRNA was significantly higher in FAD1 (2.386 ± 0.257) than IC1 (1.007 ± 0.43 , $p = 0.011$) in day 35 neurons, while there was no significant difference between FAD2 (0.888 ± 0.105) and IC2 (1.03 ± 0.087 ; $p = 0.527$). FAD1 and FAD2 *GRIA1* mRNA expression showed no significant differences from HC1 (2.622 ± 0.977 ; $p = 0.132$) and HC2 (1.197 ± 0.389 , $p = 0.795$), respectively.

Similar results were obtained from the analysis of *GRIA2* gene expression. FAD1 (2.024 ± 0.284) had significantly greater mRNA levels of *GRIA2*, compared to IC1 (1.028 ± 0.028 ; $p = 0.027$), but was not significantly different from HC1 (2.712 ± 0.941 ; $p = 0.116$). Although FAD2 (1.353 ± 0.364) had a higher mean mRNA expression of *GRIA2* compared to IC2 (1.039 ± 0.084 ; $p = 0.975$), this difference did not reach statistical significance. FAD2 was also not significantly different from HC2 (2.649 ± 0.66 , $p = 0.437$).

Regarding the relative expression of *GRIA3* mRNA, the only significant difference observed was between FAD2 (0.911 ± 0.082) and HC2 (0.277 ± 0.075 , $p = 2.34 \times 10^{-6}$), with FAD2 neurons displaying higher expression of *GRIA3*. No significant differences were detected between FAD1 (0.899 ± 0.09) and IC1 (1.014 ± 0.058 ; $p = 0.24$) or HC1 (0.804 ± 0.089 , $p = 0.325$) or between FAD2 and IC2 (1.021 ± 0.077 , $p = 0.293$).

Lastly, RT-qPCR analysis of *GRIA4* showed FAD1 (2.056 ± 0.153) mRNA levels were significantly higher than both IC1 (1.009 ± 0.045 ; $p = 3.38 \times 10^{-7}$) and HC1 (1.303 ± 0.207 , $p = 3.85 \times 10^{-5}$). For FAD2 (1.708 ± 0.182), even though there was a trend towards higher mRNA than IC2 (1.007 ± 0.043 , $p = 0.065$), this difference was not statistically significant. There was no significant difference between FAD2 and HC2 (1.977 ± 0.522 ; $p = 0.563$).

Altogether, these results showed FAD1 iPSC-derived day 35 neurons had increased *GRIA1*, *GRIA2*, and *GRIA4* mRNA expression compared to IC1, but there was no difference in *GRIA3* expression. Furthermore, no significant differences between FAD2 and IC2 were observed in *GRIA1*, *GRIA2*, *GRIA3*, or *GRIA4* mRNA expression, suggesting that transcriptional regulation of the GRIA genes cannot explain the increased calcium responses to AMPA.

Protein Expression of GluA1 and GluA2 Is Not Significantly Different between FAD and Control Neurons

Following the observed elevation in Ca^{2+} responses of FAD neurons compared to their IC neurons when treated with both glutamate and AMPA, it was hypothesised that these differences could be due to a difference in AMPAR subunit protein expression. We focused on GluA1 and GluA2 as the major AMPAR subunits in excitatory neurons. To investigate this hypothesis, total protein extraction from whole cell lysates of day 35 neurons was prepared for western blotting assays.

Western blots for all cell lines detected a strong band of approximately 100 kDa for both GluA1 and GluA2 (Figure 9A,B and Supplementary Figures S8–S11), present at their expected molecular weight. For some cell lines, a band of higher molecular weight, approximately 250 kDa, was also observed, which was not included in the quantification. Densitometry values of the bands at 100 kDa were normalised to respective total protein signals and a mean pooled sample, which were used to account for variability in protein loading and to normalise between separate blots, respectively. Linear regression analysis revealed no significant differences in GluA1 or GluA2 protein expression between FAD (FAD1— 0.802 ± 0.148 ; FAD2— 0.46 ± 0.066) and control cell lines IC (IC1— 1.1 ± 0.35 , $p = 0.515$; IC2— 0.733 ± 0.226 , $p = 0.25$) and HC (HC1— 1.261 ± 0.36 ; $p = 0.4$; HC2— 0.626 ± 0.152 , $p = 0.479$) (Figure 9C,D).

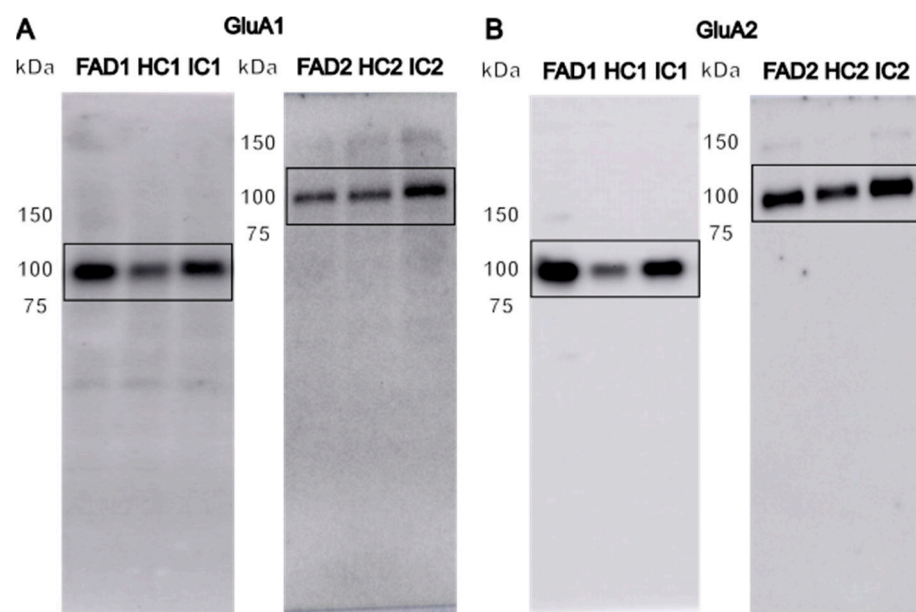


Figure 9. Cont.

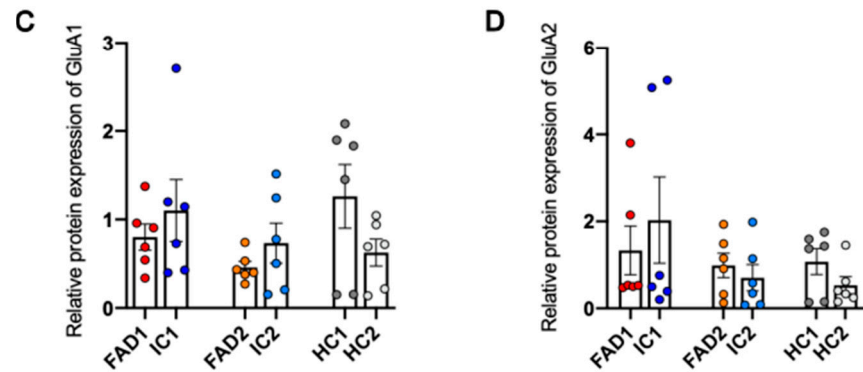


Figure 9. GluA1 and GluA2 protein expression of FAD and control neurons. Representative western blots (A,B) and relative protein expression of GluA1 (C) and GluA2 (D). Data shown are day 35 neurons; $n = 2$ replicates from 3 independent differentiations, normalised to total protein; error bars represent \pm SEM. Data are normally distributed (FAD2/HC2/IC2 GluA1) or normalised to \log_2 (FAD1/HC1/IC1 and FAD2/HC2/IC2 GluA2) or $\sqrt{\text{}}$ (FAD1/HC1/IC1 GluA1) and analysed using linear regression modelling. Independent differentiations were included as co-variables; there were no significant differences between groups. FAD—familial Alzheimer’s disease; HC—healthy control; IC—isogenic control.

These results indicate that the alterations in AMPAR Ca^{2+} signalling in FAD and control iPSC-derived neurons differentiated for 35 days were not due to differences in protein expression of GluA1 and GluA2 AMPAR subunits.

4. Discussion

Glutamate and calcium dyshomeostasis have been documented in Alzheimer’s disease; however, it has been difficult to determine whether or not calcium and glutamate phenotypes precede amyloid and tau phenotypes in humans. To address this question in a 2D human cell model of the early stages of the disease, this study aimed to generate iPSC-derived neurons from FAD patients, isogenic controls, and healthy controls and measure Ca^{2+} responses following the application of glutamate, NMDA, AMPA, and kainate. The results obtained in this study showed that day 35 FAD iPSC-derived neurons did not demonstrate evidence of AD-associated $\text{A}\beta$ and tau pathology and yet displayed altered Ca^{2+} responses. Neurons from FAD patients had elevated Ca^{2+} responses to both glutamate and AMPA but not to kainate and NMDA when compared to their isogenic controls. Together, the data suggest that mutations in *PSEN1* cause increased Ca^{2+} responses to AMPA as an early phenotype of AD.

4.1. FAD Neurons Lacking $\text{A}\beta$ and Tau Pathology Show Elevated Ca^{2+} Responses to Glutamate and AMPA Compared to Isogenic Controls

In AD, cortical brain regions are severely affected by both $\text{A}\beta$ and tau pathology and, eventually, neuronal loss. Hence, cortical glutamatergic neurons represent an appropriate model to study FAD neuronal calcium responses to excitatory stimuli.

The impact of FAD-causing mutations in the *PSEN1* gene, *PSEN1*^{S290C} and *PSEN1*^{A246E}, was investigated using iPSC-derived neurons from FAD patients as well as isogenic and healthy controls. Although the *PSEN1*^{S290C} mutation results in the deletion of exon 9, preventing the endoproteolysis of *PSEN1*, *PSEN1*^{S290C} is still generally considered to be functionally active, leading to an increased $\text{A}\beta_{42}/\text{A}\beta_{40}$ peptide ratio [52,53], similar to *PSEN1*^{A246E} [52,54]. This has been suggested to occur due to the ability of *PSEN1*^{S290C} to adopt a conformation similar to the heterodimeric active *PSEN1* as opposed to the inactive *PSEN1* holoprotein [55]. Furthermore, the pathologic function of *PSEN1*^{S290C} in generating elevated $\text{A}\beta_{42}$ levels is believed to be independent of its inability to undergo endoproteolysis but rather due to the introduction of the point mutation (S290C), which occurs as a

result of the exon 9 deletion [53]. Hence, although PSEN1^{S290C} is structurally different from PSEN1^{A246E}, it is not clear whether this results in different AD-associated phenotypes.

In this study, iPSC-derived neurons were differentiated for a total of 35 days. Changes in cell morphology from iPSCs into neurons and expression of the fluorescent reporter GFP (co-expressed with NGN2) could be observed from day 1 of neuronal differentiation. Immunocytochemistry results from this study confirmed the cell cultures generated expressed the neuronal marker MAP2, while no cells positive for the astrocytic marker GFAP were observed.

The presence of amyloid- β plaques and neurofibrillary tangles in human *postmortem* brain tissue provides the criteria for the neuropathologic diagnosis of AD [56]. Both plasma and cerebral spinal fluid levels of A β are decreased in AD and are inversely associated with plaque burden [43,44]. Since A β plaques cannot be formed in 2D neuronal cultures due to the frequent media changes, the levels of A β peptides released into the cell medium are commonly used as a measurement of A β pathology. Several long-term 2D cell culture models of AD have detected elevated A β 42/A β 40 ratios [36,47–50] or increased secreted A β 42 in the media [47], while others have found no differences [36]. This discrepancy may be explained by the use of different protocols to generate neuronal subtypes or by the length of time that neurons are cultured/matured for. Another important contributing factor is the use of cell lines harbouring different FAD mutations or sporadic AD lines bearing different genetic risk factors and their comparison with either healthy or isogenic controls. Statistical analysis of A β 42 levels for day 35 iPSC-derived neurons generated for this work showed FAD2 neurons had higher levels of A β 42 than a healthy control line HC2 but, critically, was not statistically different from its isogenic control IC2. Since healthy controls have an entirely different genome from a familial disease cell line, differences found between these cells may be biased by factors other than the disease-associated mutation and, therefore, complicate the interpretation of the results. Isogenic controls, on the other hand, should have the same genome as their parental cell line, except for the disease-causing mutation that is reverted to WT, making it a more useful comparison to understand the contribution of specific mutations to disease phenotypes. Thus, we expect to observe differences in responses between unrelated lines. Nevertheless, the inclusion of additional healthy controls is helpful to assess variations in responses. Apart from the different types of controls used, the presence of glial cells in the culture can also affect the A β phenotype, as they are involved in the clearance of this peptide [57]. Although our iPSC-derived neuronal model did not show any GFAP+ cells after immunostaining analysis, it cannot be ruled out that GFAP-negative astrocytic or other glial populations may be present in the culture and impact A β processing.

The microtubule-associated protein tau is enriched in the axons of mature neurons; however, in pathological conditions such as AD, it is hyperphosphorylated and accumulates in the cell soma and dendrites, where it forms insoluble aggregates and neurofibrillary tangles. A total of 59 tau phosphorylation sites have been detected in human *postmortem* brain tissue of AD patients [58,59], and serine 404 (p-Tau S404) is considered one of the first epitopes to be phosphorylated in the disease [51]. Tau phosphorylation at different epitopes has been previously replicated in cell models of AD, including p-Tau S404 [48], hence its inclusion as a measurement for early stages of tau pathology. However, statistical analysis revealed no significant differences in the levels of p-Tau S404 between FAD and control cell lines in day 35 neurons. Although a combination of factors, such as lipid metabolism, endocytosis, and the immune response, contribute to pathologic tau accumulation [60], elevated A β levels are also believed to accelerate tau pathology [61]. Given that an A β pathology phenotype at this stage of neuronal maturation was not observed in the FAD neurons, this may explain the absence of a tau phenotype as well. Therefore, neither A β accumulation nor increased tau phosphorylation were detected in day 35 FAD iPSC-derived neurons in this study. Thus, this model permits the study of early FAD phenotypes associated with PSEN1 mutations in human cells.

Another phenotype of AD is neuronal hyperexcitability (increased excitability), which is thought to precede neuronal hypoexcitability (reduced excitability) and cell death [32]. This elevated neuronal activity is thought to promote neurodegeneration in specific neurons [30] and correlate with cognitive decline. Numerous abnormalities have been suggested to contribute to the change in neuronal excitability, including calcium and glutamate dyshomeostasis [32]. To understand whether there is a calcium phenotype in early FAD neurons, it was first confirmed that all cell lines responded to high K^+ . HC2 neurons demonstrated greater responses to high K^+ than FAD2 neurons, suggesting HC2 may have a greater density of K^+ channels compared to FAD2 cells. This could impact neuronal differentiation and excitability, key functions of K^+ channels [62,63]. Nevertheless, no significant differences were found between the isogenic control IC2 and FAD2 neurons, suggesting the differences observed between HC2 and FAD2 lines originate from genetic differences between the cell lines unrelated to the FAD mutation. Then, to investigate how neurons respond to excitatory stimuli, the experiments aimed to measure neuronal calcium signals after treatment with glutamate and the iGluR agonists, NMDA, AMPA, and kainate. Analysis of the maximum amplitude of the calcium response to each drug revealed FAD neurons had significantly higher calcium responses to both glutamate and AMPA compared to their isogenic controls. No significant differences were observed between the disease and isogenic controls following treatment with NMDA or kainate. Although this work focused on iGluR agonists, the differences in Ca^{2+} responses to glutamate could also stem from changes in mGluR, previously shown to have altered expression and/or activity in AD [64]. Hence, future work is crucial to elucidate the contribution of mGluR to Ca^{2+} dyshomeostasis in the model studied here.

Both $A\beta$ and tau contribute to calcium dyshomeostasis and AMPAR trafficking dysfunction, resulting in a reduction in AMPAR expression and function and defective synaptic plasticity, as reviewed in [65,66]. Nevertheless, the data identified an aberrant calcium signalling phenotype that appears to occur independently of $A\beta$ or tau phenotypes. Consequently, in the absence of evidence for $A\beta$ and early phosphorylated tau S404 changes, alternative mechanisms need to be considered. Notch-1 expression is altered in neurons bearing these same *PSEN1* mutations [67]. Notch signalling is implicated in stem cell renewal, proliferation, and differentiation, as well as neuronal development [68]. Thus, reduced Notch-1 expression in FAD neurons could lead to differential regulation of AMPAR expression in FAD, control iPSC-derived neurons, and explain the phenotypes observed here.

4.2. Aberrant Ca^{2+} Signalling of FAD Neurons Occurs Independently of Changes in GluA1 and GluA2 Protein Expression

While the data failed to demonstrate alterations in GluA1 and GluA2 protein levels in FAD compared to isogenic control neurons, there were some increases in *GRIA1*, *GRIA2*, and *GRIA4* at the mRNA level. The transcriptional regulatory mechanisms were not assessed since the transcriptional up-regulation did not lead to concomitant increases in protein levels. AMPAR are tetrameric assemblies of GluA1-GluA4 subunits that permit Na^+ and Ca^{2+} influx into the cells. Ca^{2+} -permeable AMPAR is important for long-term potentiation (LTP) induction and long-term memory formation [69]. The permeability of AMPARs to Ca^{2+} depends on subunit composition, and GluA2 subunit permeability to Ca^{2+} is regulated by RNA editing. The post-transcriptional modification of *GRIA2* RNA from a codon encoding glutamine (Q) to a codon encoding arginine (R) renders this subunit impermeable to Ca^{2+} . Thus, AMPARs lacking GluA2 or containing the unedited version of GluA2 are Ca^{2+} permeable [70]. The unedited *GRIA2* mRNA has very low expression in the adult human brain, comprising less than 10% of *GRIA2* in the white matter and less than 1% in the grey matter [71]. In spite of its low expression, unedited GluA2 can contribute to synaptic plasticity and excitotoxic neuronal cell death, as reviewed in [72]. Interestingly, lower RNA editing of GluA2 has been reported in AD brains [73–75]. Although RT-qPCR of *GRIA2* performed in this study is insufficient to discern edited from unedited *GRIA2*, previous studies have employed different strategies, such as restriction

enzyme digestion and Sanger sequencing of PCR products [76,77], to quantify unedited *GRIA2* mRNA. Future work utilising these assays could inform whether changes in the amount of edited or unedited *GRIA2* occur in FAD neurons.

The expression of AMPAR subunits varies across regions of the mammalian brain. In murine hippocampal synapses, the majority of AMPARs are comprised of GluA1/2 subunits, followed by a smaller fraction of GluA2/3 heterodimers [78,79]. In the adult rat cortex, GluA1 is the predominant subunit (~45% of total AMPAR), followed by GluA2 (21%), GluA3 (27%), and very low levels of GluA4 (less than 6%) [13]. Several studies have shown GluA1 and GluA2 protein expression is decreased in AD *postmortem* brain tissue, as summarised in [29]. Lower expression of GluA1 has been reported in the frontal cortex [80–82] and cerebellum [83] of AD brains, while no differences were observed in the temporal cortex compared to healthy individuals [69], suggesting there is a brain region-specific phenotype. Regarding GluA2, this AMPAR subunit has been the most extensively studied in AD. A recent compilation of 38 proteomic studies of AD reported a total of 12 studies where GluA2 protein expression was reduced in the frontal, entorhinal, and parahippocampal cortex, as well as the hippocampus and precuneus brain regions of AD brains [29]. Most of the studies (7 out of 12) found these changes in the frontal cortex. Nonetheless, contrasting results have been reported by a couple of studies that detected an upregulation of GluA2 protein expression in the temporal cortex and hippocampus of AD patients [69,84]. The work conducted by Barbour and colleagues [69] is the only study to examine GluA2 expression in the temporal cortex, indicating GluA2 could be differentially regulated in specific brain regions; however, more studies analysing this area of the brain are required to confirm these results. While Stepler et al. [85] found decreased levels of GluA2 in tissue homogenates of the whole hippocampus, Yeung et al. [84] found GluA2 expression was elevated in a subregion of the hippocampus, the stratum moleculare layer of the dentate gyrus, but no significant changes were detected in the stratum granulosum and hilus areas of the dentate gyrus, or in any of the CA1, CA2, or CA3 regions of the hippocampus. Also, no changes were observed in the superior temporal gyrus, subiculum, and entorhinal cortex of AD versus control donors. Thus, a potential explanation for these discrepancies is that GluA2 expression is differentially altered in specific subregions of the hippocampus. Furthermore, although the *postmortem* brain tissue used by Yeung et al. [84] was obtained from a brain bank located in New Zealand, the ethnicity of their cohort was not specified. In contrast, Stepler et al. [85] analysed brains from African American and non-Hispanic White individuals and identified 185 proteins differentially expressed in these two groups. African American and Hispanic populations have a greater risk of developing AD and non-AD dementia than non-Hispanic white adults; however, these groups are commonly underrepresented in proteomic studies of AD. Even though GluA4 was not differentially expressed between the two ethnicity groups included in this study, these results highlight the need for more research, including ethnically diverse cohorts. This will allow for a better understanding of variabilities in disease-associated phenotypes among different populations so that future therapies can target various ethnic groups.

Overall, the work of Askenazi et al. (2023) [29], compiling studies on AD proteome alterations, postulates that expression of GluA1 and GluA2 is reduced in later stages of AD. Interestingly, this phenotype is not observed in studies of the early stages of the disease, including our study, in which western blot analysis showed no changes in total cell protein expression of GluA1 and GluA2. Since the AD model presented here represents an early stage of the disease, preceding A β and tau phenotypes, it can be speculated that abnormalities in AMPAR protein levels have not yet developed at this stage.

In this study, protein expression of GluA3 and GluA4 in iPSC-derived neurons was not analysed, but changes in their expression have been reported in AD *postmortem* brain tissue. GluA3 and GluA4 follow a similar pattern of protein expression as those observed for GluA1 and GluA2. Even though no changes were detected in the early stages of the disease, lower levels of GluA3 were found in the hippocampus, precuneus, frontal, and entorhinal cortex in the late stages of AD pathology [29]. Despite the low number of

studies on GluA4, decreased expression of this subunit has been reported in the frontal and entorhinal cortex of advanced stages of AD [86,87]. Thus, future work measuring GluA3 and GluA4 protein levels in day 35 iPSC-derived neurons is required to fully characterise the protein expression of AMPAR subunits in this model. In summary, *postmortem* brain tissue of AD patients shows reduced AMPAR expression, but these changes are only observed in the late/end stages of the disease. Likewise, the results from this study found no differences in total protein levels of GluA1 and GluA2 subunits in FAD iPSC-derived neurons representing early stages of pathology compared to isogenic controls. This suggests the mechanism leading to changes in how FAD neurons respond to AMPA, compared to controls, is not explained by alterations in the total cellular protein expression of these two subunits. Nonetheless, analysis of total cellular protein expression may mask changes in protein expression in specific cellular compartments. The expression of AMPARs in the plasma membrane, specifically, is crucial for receptor function and can be regulated through post-translational modifications. Reversible post-translational modifications, such as phosphorylation, palmitoylation, and ubiquitination, affect receptor subunit exocytosis, endocytosis, degradation, and gating [88]. Phosphorylation of GluA1 regulates synaptic plasticity by potentiating AMPAR responses to glutamate [89] and increasing channel conductance [90] and open probability [91]. While phosphorylation of GluA1 at epitopes S818, S831, and S845 promotes synaptic insertion of AMPAR and dephosphorylation causes endocytosis, dephosphorylation of GluA1 at S567 increases receptor expression at the synapse [88]. GluA2 phosphorylation, on the other hand, is required for AMPAR internalisation in the CA1 region of the hippocampus both *in vitro* and *in vivo* [92,93].

Ubiquitination comprises the attachment of a single ubiquitin or polymeric ubiquitin chains to the lysine residues of a substrate protein [94]. All AMPAR subunits can undergo ubiquitination when treated with AMPA [95]. This post-translational modification is calcium-dependent [95,96] and only occurs in receptors present in the plasma membrane [95]. The ubiquitination of AMPAR signals for lysosomal [96,97] or proteasomal degradation [98] of this receptor, and most studies report it also regulates endocytosis [96,98,99]. Importantly, ubiquitination of AMPAR also modulates synaptic transmission [96,98–100]. In rat neuronal cultures, AMPA treatment increases the number of internalised GluA1. This phenotype is abolished in GluA1 mutants lacking ubiquitination sites. Instead, mutant GluA1 shows reduced GluA1 degradation and internalisation and increased GluA1 expression at the cell surface [96,98]. Finally, human *postmortem* brain tissue of AD patients showed increased expression of ubiquitinated GluA1 protein, suggesting ubiquitination of AMPAR subunits may play an important role in modulating plasma membrane expression and function. Proteins can also be modified by being covalently bound to lipids, such as fatty acids. This process is termed fatty acylation and includes the post-translational modification palmitoylation, which is the addition of the 16-carbon saturated fatty acid palmitate to one or more intracellular cysteine residues of target proteins. All four AMPAR subunits can be palmitoylated, and they are differentially regulated depending on the site of palmitoylation [101]. In HEK293T cells and primary cortical neurons, palmitoylation of cysteines in the transmembrane domain 2 of GluA1 or GluA2 accumulates these subunits in the Golgi and reduces their surface expression. C-terminal palmitoylation of AMPAR, on the other hand, does not influence steady-state surface expression of this receptor but increases its internalisation after NMDA or AMPA stimulation [101,102]. A knock-in GluA1 C811 palmitoylation-deficient mouse model (GluA1C811S) showed elevated expression of GluA1 in the cortex [103]. Altogether, these studies demonstrate that various post-translational changes to AMPARs influence their trafficking and consequent membrane expression and receptor function. Hence, future work needs to be conducted to measure the expression of all AMPAR subunits intracellularly and in the plasma membrane and to measure post-translational changes that may regulate their trafficking to and from the membrane.

Apart from AMPAR regulation via post-translational modifications, the composition of the lipid membrane, where AMPARs are embedded, provides another layer of ion channel

modulation. Presynaptic and postsynaptic membranes are enriched in cholesterol, a sterol lipid that has been linked to AD. Although cholesterol does not affect AMPA binding to its receptor [104], it can still modulate AMPAR activity. Analysis of intracellular calcium levels in cultures of rat hippocampal neurons demonstrated that cholesterol depletion decreased AMPAR-mediated calcium influx [105]. In rat hippocampal slices, cholesterol depletion reduced both the amplitude of AMPAR-mediated excitatory postsynaptic currents (EPSCs) [106] and basal synaptic transmission [105]. Using the same model, it was shown that AMPA treatment potentiated basal synaptic transmission in both normal and cholesterol-depleted conditions. However, in the absence of cholesterol, this potentiation lasted for a shorter period, and the responses to AMPA were not fully abolished after washing out the drug, as was the case for control slices [105]. Nevertheless, contrasting results were found in rat cerebellar granule cells and mouse cortical neurons, where cholesterol depletion reduced NMDA-evoked currents but had no effect on AMPAR-mediated currents [107,108]. This divergence could possibly be explained by the different cell types analysed, the concentration and duration of the stimulus, or the AMPAR agonist utilised by each study. Hence, further investigation is required to understand the effect of neuronal membrane cholesterol content on AMPAR function.

The poly-unsaturated fatty acid arachidonic acid (AA) has also been implicated in neuronal excitability. Mouse brain slices expressing human APP (hAPP) showed higher surface expression of GluA1 and GluA2 subunits of AMPARs when treated with AA, which resulted in increased neuronal activity. AA is generated from the hydrolysis of phospholipids by phospholipase-A2 (PLA₂), an enzyme that was hyperphosphorylated in hAPP animals, suggesting elevated activation [109]. To confirm this hypothesis, the authors blocked PLA₂ activity, which prevented the increase in AMPAR protein expression as well as neuronal hyperactivity. PLA₂ further acts in synaptic transmission by increasing AMPA affinity, binding to its receptor [110], and modulating AMPAR phosphorylation [111]. In rat brain slices, inhibition of calcium-independent PLA₂ increased GluA1 phosphorylation at residue S831, while inhibition of calcium-dependent PLA₂ enhanced phosphorylation of GluA2/3 at S880/891 [111]. Although the authors did not investigate the impact of AMPAR phosphorylation on neuronal activity, it is possible that it could affect AMPAR trafficking and expression.

5. Future Directions

In this study, iPSC-derived neurons from FAD patients bearing *PSEN1* mutations showed greater calcium responses to glutamate and AMPA than isogenic control neurons. This occurred in the absence of overt A β 42 and tau S404 phosphorylation phenotypes or changes in total cellular protein expression of GluA1 and GluA2 subunits of AMPAR. Future work should measure total cellular protein expression of GluA3 and GluA4 subunits, as well as expression of all AMPAR subunits in the neuronal membrane and intracellular compartments separately. Trafficking of AMPARs to the membrane can be regulated by post-translational modifications such as phosphorylation, ubiquitylation, and palmitoylation; thus, investigating levels of these post-translational modifications to AMPAR subunits and the enzymes involved in these pathways could demonstrate the mechanisms promoting early calcium signalling dysfunction in FAD neurons.

6. Conclusions

The iPSC-derived cortical excitatory neurons from FAD patients display elevated calcium responses to glutamate and AMPA compared to their isogenic controls. This early calcium phenotype was observed in the absence of an A β or tau phenotype. Although mRNA levels of the AMPAR subunits *GRIA1*, *GRIA2*, and *GRIA4* were increased in FAD1 neurons compared to IC1 neurons, this difference was not significant between FAD2 and IC2 neurons. Furthermore, protein expression of the AMPAR subunits GluA1 and GluA2 was not significantly different between FAD and isogenic control neurons. Hence, the

difference in how FAD neurons respond to AMPA cannot be explained by changes in total cellular protein expression of AMPAR subunits GluA1 or GluA2.

Supplementary Materials: The following supporting information can be downloaded at: <https://www.mdpi.com/article/10.3390/life14050625/s1>, Figure S1: Representative images and timeline of differentiation, Figure S2: Representative images of no primary antibody control for immunostaining from FAD1, IC1 and HC1, Figure S3: Representative images of no primary antibody control for immunostaining from FAD2, IC2 and HC2, Figure S4: Sample description and images of full membranes for Tau-5 antibody and total protein for FAD1/HC1/IC1, Figure S5: Sample description and images of full membranes for Tau-5 antibody and total protein for FAD2/HC2/IC2, Figure S6: Sample description and images of full membranes for p-Tau-s404 antibody and total protein for FAD1/HC1/IC1, Figure S7: Sample description and images of full membranes for p-Tau-s404 antibody and total protein for FAD2/HC2/IC2, Figure S8: Sample description and images of full membranes for GluA1 antibody and total protein for FAD1/HC1/IC1, Figure S9: Sample description and images of full membranes for GluA1 antibody and total protein for FAD2/HC2/IC2, Figure S10: Sample description and images of full membranes for GluA2 antibody and total protein for FAD1/HC1/IC1, Figure S11: Sample description and images of full membranes for GluA2 antibody and total protein for FAD2/HC2/IC2.

Author Contributions: Conceptualization, H.T.D.A. and L.O.; methodology, H.T.D.A. and N.M.; formal analysis, H.T.D.A.; resources, L.O.; data curation, H.T.D.A.; writing—original draft preparation, H.T.D.A.; writing—review and editing, H.T.D.A., N.M., and L.O.; supervision, N.M. and L.O.; project administration, L.O.; funding acquisition, L.O. All authors have read and agreed to the published version of the manuscript.

Funding: This research was funded by a National Health and Medical Research Council of Australia (NHMRC) Boosting Dementia Research Leadership Fellowship awarded to L.O., grant number APP1135720.

Institutional Review Board Statement: The study was conducted in accordance with the Declaration of Helsinki and approved by the University of Wollongong Human Research Ethics Committee (protocol code 13/299, 2013).

Informed Consent Statement: Informed consent was obtained from all subjects involved in the study.

Data Availability Statement: Data are available upon request.

Acknowledgments: The authors wish to acknowledge the participants, without whom this research would not be possible.

Conflicts of Interest: The authors declare no conflicts of interest.

References

- Bird, T.D. Alzheimer Disease Overview. In *GeneReviews*[®] [Internet]; University of Washington: Seattle, WA, USA, 1998.
- Blacker, D.; Tanzi, R.E. The Genetics of Alzheimer Disease: Current Status and Future Prospects. *Arch. Neurol.* **1998**, *55*, 294–296. [[CrossRef](#)] [[PubMed](#)]
- Glennner, G.G.; Wong, C.W. Alzheimer's Disease: Initial Report of the Purification and Characterization of a Novel Cerebrovascular Amyloid Protein. *Biochem. Biophys. Res. Commun.* **1984**, *120*, 885–890. [[CrossRef](#)] [[PubMed](#)]
- Brion, J.P.; Couck, A.M.; Passareiro, E.; Flament-Durand, J. Neurofibrillary Tangles of Alzheimer's Disease: An Immunohistochemical Study. *J. Submicrosc. Cytol.* **1985**, *17*, 89–96. [[PubMed](#)]
- Ge, M.; Zhang, J.; Chen, S.; Huang, Y.; Chen, W.; He, L.; Zhang, Y. Role of Calcium Homeostasis in Alzheimer's Disease. *Neuropsychiatr. Dis. Treat.* **2022**, *18*, 487–498. [[CrossRef](#)]
- Bezprozvanny, I.; Mattson, M.P. Neuronal Calcium Mishandling and the Pathogenesis of Alzheimer's Disease. *Trends Neurosci.* **2008**, *31*, 454–463. [[CrossRef](#)] [[PubMed](#)]
- Zhang, H.; Sun, S.; Herreman, A.; De Strooper, B.; Bezprozvanny, I. Role of Presenilins in Neuronal Calcium Homeostasis. *J. Neurosci.* **2010**, *30*, 8566–8580. [[CrossRef](#)] [[PubMed](#)]
- Tu, H.; Nelson, O.; Bezprozvanny, A.; Wang, Z.; Lee, S.F.; Hao, Y.H.; Serneels, L.; De Strooper, B.; Yu, G.; Bezprozvanny, I. Presenilins form ER Ca²⁺ Leak Channels, a Function Disrupted by Familial Alzheimer's Disease-Linked Mutations. *Cell* **2006**, *126*, 981–993. [[CrossRef](#)]
- Green, K.N.; Demuro, A.; Akbari, Y.; Hitt, B.D.; Smith, I.F.; Parker, I.; LaFerla, F.M. SERCA Pump Activity Is Physiologically Regulated by Presenilin and Regulates Amyloid β Production. *J. Cell Biol.* **2008**, *181*, 1107–1116. [[CrossRef](#)]

10. Cheung, K.-H.; Shineman, D.; Müller, M.; Cárdenas, C.; Mei, L.; Yang, J.; Tomita, T.; Iwatsubo, T.; Lee, V.M.-Y.; Foscett, J.K. Supplemental Data—Mechanism of Ca²⁺ Disruption in Alzheimer’s Disease by Presenilin Regulation of InsP3 Receptor Channel Gating. *Neuron* **2008**, *58*, 871–883. [[CrossRef](#)]
11. Lee, J.H.; McBrayer, M.K.; Wolfe, D.M.; Haslett, L.J.; Kumar, A.; Sato, Y.; Lie, P.P.Y.; Mohan, P.; Coffey, E.E.; Kompella, U.; et al. Presenilin 1 Maintains Lysosomal Ca²⁺ Homeostasis by Regulating VAMPase-Mediated Lysosome Acidification. *Cell Rep.* **2015**, *12*, 1430. [[CrossRef](#)]
12. Wisden, W.; Seeburg, P.H. Mammalian Ionotropic Glutamate Receptors. *Curr. Opin. Neurobiol.* **1993**, *3*, 291–298. [[CrossRef](#)]
13. Schwenk, J.; Baehrens, D.; Haupt, A.; Bildl, W.; Boudkkazi, S.; Roeper, J.; Fakler, B.; Schulte, U. Regional Diversity and Developmental Dynamics of the AMPA-Receptor Proteome in the Mammalian Brain. *Neuron* **2014**, *84*, 41–54. [[CrossRef](#)] [[PubMed](#)]
14. Hsieh, H.; Boehm, J.; Sato, C.; Iwatsubo, T.; Tomita, T.; Sisodia, S.; Malinow, R. AMPAR Removal Underlies Aβ-Induced Synaptic Depression and Dendritic Spine Loss. *Neuron* **2006**, *52*, 831–843. [[CrossRef](#)]
15. Whitcomb, D.J.; Hogg, E.L.; Regan, P.; Piers, T.; Narayan, P.; Whitehead, G.; Winters, B.L.; Kim, D.H.; Kim, E.; St George-Hyslop, P.; et al. Intracellular Oligomeric Amyloid-Beta Rapidly Regulates GluA1 Subunit of AMPA Receptor in the Hippocampus. *Sci. Rep.* **2015**, *5*, 10934. [[CrossRef](#)]
16. Hoover, B.R.; Reed, M.N.; Su, J.; Penrod, R.D.; Kotilinek, L.A.; Grant, M.K.; Pitstick, R.; Carlson, G.A.; Lanier, L.M.; Yuan, L.L.; et al. Tau Mislocalization to Dendritic Spines Mediates Synaptic Dysfunction Independently of Neurodegeneration. *Neuron* **2010**, *68*, 1067–1081. [[CrossRef](#)] [[PubMed](#)]
17. Paoletti, P. Molecular Basis of NMDA Receptor Functional Diversity. *Eur. J. Neurosci.* **2011**, *33*, 1351–1365. [[CrossRef](#)]
18. Sun, X.-Y.; Tuo, Q.-Z.; Liuyang, Z.-Y.; Xie, A.-J.; Feng, X.-L.; Yan, X.; Qiu, M.; Li, S.; Wang, X.-L.; Cao, F.-Y.; et al. Extrasynaptic NMDA Receptor-Induced Tau Overexpression Mediates Neuronal Death through Suppressing Survival Signaling ERK Phosphorylation. *Cell Death Dis.* **2016**, *7*, e2449. [[CrossRef](#)] [[PubMed](#)]
19. Lesné, S.; Ali, C.; Gabriel, C.; Croci, N.; MacKenzie, E.T.; Glabe, C.G.; Plotkine, M.; Marchand-Verrecchia, C.; Vivien, D.; Buisson, A. NMDA Receptor Activation Inhibits α-Secretase and Promotes Neuronal Amyloid-β Production. *J. Neurosci.* **2005**, *25*, 9367–9377. [[CrossRef](#)]
20. Bordji, K.; Becerril-Ortega, J.; Nicole, O.; Buisson, A. Activation of Extrasynaptic, But Not Synaptic, NMDA Receptors Modifies Amyloid Precursor Protein Expression Pattern and Increases Amyloid-β Production. *J. Neurosci.* **2010**, *30*, 15927–15942. [[CrossRef](#)]
21. Li, S.; Hong, S.; Shepardson, N.E.; Walsh, D.M.; Shankar, G.M.; Selkoe, D. Soluble Oligomers of Amyloid β Protein Facilitate Hippocampal Long-Term Depression by Disrupting Neuronal Glutamate Uptake. *Neuron* **2009**, *62*, 788–801. [[CrossRef](#)]
22. Arias, C.; Arrieta, I.; Tapia, R. B-Amyloid Peptide Fragment 25–35 Potentiates the Calcium-dependent Release of Excitatory Amino Acids from Depolarized Hippocampal Slices. *J. Neurosci. Res.* **1995**, *41*, 561–566. [[CrossRef](#)]
23. Parpura-Gill, A.; Beitz, D.; Uemura, E. The Inhibitory Effects of β-Amyloid on Glutamate and Glucose Uptakes by Cultured Astrocytes. *Brain Res.* **1997**, *754*, 65–71. [[CrossRef](#)] [[PubMed](#)]
24. Snyder, E.M.; Nong, Y.; Almeida, C.G.; Paul, S.; Moran, T.; Choi, E.Y.; Nairn, A.C.; Salter, M.W.; Lombroso, P.J.; Gouras, G.K.; et al. Regulation of NMDA Receptor Trafficking by Amyloid-β. *Nat. Neurosci.* **2005**, *8*, 1051–1058. [[CrossRef](#)]
25. Winslow, B.T.; Onysko, M.K.; Stob, C.M.; Hazlewood, K.A. Treatment of Alzheimer Disease. *Am. Fam. Physician* **2011**, *83*, 1403–1412. [[CrossRef](#)] [[PubMed](#)]
26. Falcón-Moya, R.; Sihra, T.S.; Rodríguez-Moreno, A. Kainate Receptors: Role in Epilepsy. *Front. Mol. Neurosci.* **2018**, *11*, 217. [[CrossRef](#)]
27. Barthet, G.; Moreira-De-Sá, A.; Zhang, P.; Deforges, S.; Castanheira, J.; Gorlewicz, A.; Mülle, C. Presenilin and APP Regulate Synaptic Kainate Receptors. *J. Neurosci.* **2022**, *42*, 9253–9262. [[CrossRef](#)]
28. Malenka, R.C.; Bear, M.F. LTP and LTD: An Embarrassment of Riches. *Neuron* **2004**, *44*, 5–21. [[CrossRef](#)]
29. Askenazi, M.; Kavanagh, T.; Pires, G.; Ueberheide, B.; Wisniewski, T.; Drummond, E. Compilation of All Known Protein Changes in the Human Alzheimer’s Disease Brain. *bioRxiv* **2023**. [[CrossRef](#)]
30. Choi, D.W. Glutamate Neurotoxicity and Diseases of the Nervous System. *Neuron* **1988**, *1*, 623–634. [[CrossRef](#)] [[PubMed](#)]
31. Cox, M.F.; Hascup, E.R.; Bartke, A.; Hascup, K.N. Friend or Foe? Defining the Role of Glutamate in Aging and Alzheimer’s Disease. *Front. Aging* **2022**, *3*, 65. [[CrossRef](#)]
32. Targa Dias Anastacio, H.; Matosin, N.; Ooi, L. Neuronal Hyperexcitability in Alzheimer’s Disease: What Are the Drivers behind This Aberrant Phenotype? *Transl. Psychiatry* **2022**, *12*, 257. [[CrossRef](#)] [[PubMed](#)]
33. Celone, K.A.; Calhoun, V.D.; Dickerson, B.C.; Atri, A.; Chua, E.F.; Miller, S.L.; DePeau, K.; Rentz, D.M.; Selkoe, D.J.; Blacker, D.; et al. Alterations in Memory Networks in Mild Cognitive Impairment and Alzheimer’s Disease: An Independent Component Analysis. *J. Neurosci.* **2006**, *26*, 10222–10231. [[CrossRef](#)] [[PubMed](#)]
34. Dickerson, B.C.; Salat, D.H.; Greve, D.N.; Chua, E.F.; Rand-Giovannetti, E.; Rentz, D.M.; Bertram, L.; Mullin, K.; Tanzi, R.E.; Blacker, D.; et al. Increased Hippocampal Activation in Mild Cognitive Impairment Compared to Normal Aging and AD. *Neurology* **2005**, *65*, 404–411. [[CrossRef](#)] [[PubMed](#)]
35. Balez, R.; Ooi, L. Getting to NO Alzheimer’s Disease: Neuroprotection versus Neurotoxicity Mediated by Nitric Oxide. *Oxid. Med. Cell. Longev.* **2016**, *2016*, 3806157. [[CrossRef](#)]

36. Ghatak, S.; Dolatabadi, N.; Trudler, D.; Zhang, X.; Wu, Y.; Mohata, M.; Ambasadhan, R.; Talantova, M.; Lipton, S.A. Mechanisms of Hyperexcitability in Alzheimer's Disease iPSC-Derived Neurons and Cerebral Organoids vs. Isogenic Control. *eLife* **2019**, *8*, e50333. [[CrossRef](#)] [[PubMed](#)]
37. Šišková, Z.; Justus, D.; Kaneko, H.; Friedrichs, D.; Henneberg, N.; Beutel, T.; Pitsch, J.; Schoch, S.; Becker, A.; VonderKammer, H.; et al. Dendritic Structural Degeneration Is Functionally Linked to Cellular Hyperexcitability in a Mouse Model of Alzheimer's Disease. *Neuron* **2014**, *84*, 1023–1033. [[CrossRef](#)]
38. Lerdkrai, C.; Asavapanumas, N.; Brawek, B.; Kovalchuk, Y.; Mojtahedi, N.; Del Moral, M.O.; Garaschuk, O. Intracellular Ca²⁺ Stores Control in Vivo Neuronal Hyperactivity in a Mouse Model of Alzheimer's Disease. *Proc. Natl. Acad. Sci. USA* **2018**, *115*, E1279–E1288. [[CrossRef](#)] [[PubMed](#)]
39. Maksour, S.; Finol-Urdaneta, R.K.; Hulme, A.J.; Castro Cabral-da-Silva, M.; Targa Dias Anastacio, H.; Balez, R.; Berg, T.; Turner, C.; Sanz, S.; Engel, M.; et al. Alzheimer's Disease Induced Neurons Bearing PSEN1 Mutations Exhibit Reduced Excitability. *bioRxiv* **2024**. [[CrossRef](#)]
40. Engel, M.; Balez, R.; Muñoz, S.S.; Cabral-da-Silva, M.C.; Stevens, C.H.; Bax, M.; Do-Ha, D.; Sidhu, K.; Sachdev, P.; Ooi, L. Viral-Free Generation and Characterization of a Human Induced Pluripotent Stem Cell Line from Dermal Fibroblasts. *Stem Cell Res.* **2018**, *32*, 135–138. [[CrossRef](#)]
41. Muñoz, S.S.; Balez, R.; Castro Cabral-da-Silva, M.E.; Berg, T.; Engel, M.; Bax, M.; Do-Ha, D.; Stevens, C.H.; Greenough, M.; Bush, A.; et al. Generation and Characterization of Human Induced Pluripotent Stem Cell Lines from a Familial Alzheimer's Disease PSEN1 A246E Patient and a Non-Demented Family Member Bearing Wild-Type PSEN1. *Stem Cell Res.* **2018**, *31*, 227–230. [[CrossRef](#)]
42. Nehme, R.; Zuccaro, E.; Ghosh, S.D.; Li, C.; Sherwood, J.L.; Pietilainen, O.; Barrett, L.E.; Limone, F.; Worringer, K.A.; Kommineni, S.; et al. Combining NGN2 Programming with Developmental Patterning Generates Human Excitatory Neurons with NMDAR-Mediated Synaptic Transmission. *Cell Rep.* **2018**, *23*, 2509–2523. [[CrossRef](#)] [[PubMed](#)]
43. Hansson, O.; Lehmann, S.; Otto, M.; Zetterberg, H.; Lewczuk, P. Advantages and Disadvantages of the Use of the CSF Amyloid β (A β) 42/40 Ratio in the Diagnosis of Alzheimer's Disease. *Alzheimer's Res. Ther.* **2019**, *11*, 34. [[CrossRef](#)]
44. Schindler, S.E.; Bollinger, J.G.; Ovod, V.; Mawuenyega, K.G.; Li, Y.; Gordon, B.A.; Holtzman, D.M.; Morris, J.C.; Benzinger, T.L.S.; Xiong, C.; et al. High-Precision Plasma β -Amyloid 42/40 Predicts Current and Future Brain Amyloidosis. *Neurology* **2019**, *93*, e1647. [[CrossRef](#)] [[PubMed](#)]
45. Amft, M.; Ortner, M.; Eichenlaub, U.; Goldhardt, O.; Diehl-Schmid, J.; Hedderich, D.M.; Yakushev, I.; Grimmer, T. The Cerebrospinal Fluid Biomarker Ratio A β 42/40 Identifies Amyloid Positron Emission Tomography Positivity Better than A β 42 Alone in a Heterogeneous Memory Clinic Cohort. *Alzheimer's Res. Ther.* **2022**, *14*, 60. [[CrossRef](#)] [[PubMed](#)]
46. Hansson, O.; Zetterberg, H.; Buchhave, P.; Andreasson, U.; Londos, E.; Minthon, L.; Blennow, K. Prediction of Alzheimer's Disease Using the CSF A β 42/A β 40 Ratio in Patients with Mild Cognitive Impairment. *Dement. Geriatr. Cogn. Disord.* **2007**, *23*, 316–320. [[CrossRef](#)] [[PubMed](#)]
47. Balez, R.; Steiner, N.; Engel, M.; Muñoz, S.S.; Lum, J.S.; Wu, Y.; Wang, D.; Vallotton, P.; Sachdev, P.; O'Connor, M.; et al. Neuroprotective Effects of Apigenin against Inflammation, Neuronal Excitability and Apoptosis in an Induced Pluripotent Stem Cell Model of Alzheimer's Disease. *Sci. Rep.* **2016**, *6*, 31450. [[CrossRef](#)] [[PubMed](#)]
48. Balez, R.; Stevens, C.H.; Lenk, K.; Sidhu, K.; Sutherland, G.; Ooi, L. Increased Neuronal Nitric Oxide Synthase in Alzheimer's Disease Mediates Spontaneous Calcium Signalling and Divergent Glutamatergic Calcium Responses. *Antioxid. Redox Signal.* **2024**, *1*–23. [[CrossRef](#)]
49. Lin, Y.T.; Seo, J.; Gao, F.; Feldman, H.M.; Wen, H.L.; Penney, J.; Cam, H.P.; Gjoneska, E.; Raja, W.K.; Cheng, J.; et al. APOE4 Causes Widespread Molecular and Cellular Alterations Associated with Alzheimer's Disease Phenotypes in Human iPSC-Derived Brain Cell Types. *Neuron* **2018**, *98*, 1141–1154.e7. [[CrossRef](#)]
50. Yang, J.; Zhao, H.; Ma, Y.; Shi, G.; Song, J.; Tang, Y.; Li, S.; Li, T.; Liu, N.; Tang, F.; et al. Early Pathogenic Event of Alzheimer's Disease Documented in iPSCs from Patients with PSEN1 Mutations. *Oncotarget* **2017**, *8*, 7900–7913. [[CrossRef](#)]
51. Mondragón-Rodríguez, S.; Perry, G.; Luna-Muñoz, J.; Acevedo-Aquino, M.C.; Williams, S. Phosphorylation of Tau Protein at Sites Ser396-404 Is One of the Earliest Events in Alzheimer's Disease and Down Syndrome. *Neuropathol. Appl. Neurobiol.* **2014**, *40*, 121–135. [[CrossRef](#)]
52. Borchelt, D.R.; Thinakaran, G.; Eckman, C.B.; Lee, M.K.; Davenport, F.; Ratovitsky, T.; Prada, C.M.; Kim, G.; Seekins, S.; Yager, D.; et al. Familial Alzheimer's Disease-Linked Presenilin I Variants Elevate A β 1-42/1-40 Ratio in Vitro and in Vivo. *Neuron* **1996**, *17*, 1005–1013. [[CrossRef](#)]
53. Steiner, H.; Romig, H.; Grim, M.G.; Philipp, U.; Pesold, B.; Citron, M.; Baumeister, R.; Haass, C. The Biological and Pathological Function of the Presenilin-1 Δ exon 9 Mutation Is Independent of Its Defect to Undergo Proteolytic Processing. *J. Biol. Chem.* **1999**, *274*, 7615–7618. [[CrossRef](#)] [[PubMed](#)]
54. Murayama, O.; Tomita, T.; Nihonmatsu, N.; Murayama, M.; Sun, X.; Honda, T.; Iwatsubo, T.; Takashima, A. Enhancement of Amyloid β 42 Secretion by 28 Different Presenilin 1 Mutations of Familial Alzheimer's Disease. *Neurosci. Lett.* **1999**, *265*, 61–63. [[CrossRef](#)] [[PubMed](#)]
55. Berezovska, O.; Lleo, A.; Herl, L.D.; Frosch, M.P.; Stern, E.A.; Bacskai, B.J.; Hyman, B.T. Familial Alzheimer's Disease Presenilin 1 Mutations Cause Alterations in the Conformation of Presenilin and Interactions with Amyloid Precursor Protein. *J. Neurosci.* **2005**, *25*, 3009–3017. [[CrossRef](#)]

56. Hyman, B.T.; Phelps, C.H.; Beach, T.G.; Bigio, E.H.; Cairns, N.J.; Carrillo, M.C.; Dickson, D.W.; Duyckaerts, C.; Frosch, M.P.; Masliah, E.; et al. National Institute on Aging–Alzheimer’s Association Guidelines for the Neuropathologic Assessment of Alzheimer’s Disease. *Alzheimers. Dement.* **2012**, *8*, 1. [[CrossRef](#)]
57. Ries, M.; Sastre, M. Mechanisms of A β clearance and degradation by glial cells. *Front. Aging Neurosci.* **2016**, *8*, 160. [[CrossRef](#)]
58. Xia, Y.; Prokop, S.; Giasson, B.I. “Don’t Phos Over Tau”: Recent Developments in Clinical Biomarkers and Therapies Targeting Tau Phosphorylation in Alzheimer’s Disease and Other Tauopathies. *Mol. Neurodegener.* **2021**, *16*, 37. [[CrossRef](#)]
59. Wesseling, H.; Mair, W.; Kumar, M.; Schlawfner, C.N.; Tang, S.; Beerepoot, P.; Fatou, B.; Guise, A.J.; Cheng, L.; Takeda, S.; et al. Tau PTM Profiles Identify Patient Heterogeneity and Stages of Alzheimer’s Disease. *Cell* **2020**, *183*, 1699–1713.e13. [[CrossRef](#)]
60. van der Kant, R.; Goldstein, L.S.B.; Ossenkoppele, R. Amyloid- β -Independent Regulators of Tau Pathology in Alzheimer Disease. *Nat. Rev. Neurosci.* **2020**, *21*, 21–35. [[CrossRef](#)] [[PubMed](#)]
61. Kwak, S.S.; Washicosky, K.J.; Brand, E.; von Maydell, D.; Aronson, J.; Kim, S.; Capen, D.E.; Cetinbas, M.; Sadreyev, R.; Ning, S.; et al. Amyloid-B42/40 Ratio Drives Tau Pathology in 3D Human Neural Cell Culture Models of Alzheimer’s Disease. *Nat. Commun.* **2020**, *11*, 1377. [[CrossRef](#)]
62. Spitzer, N.C.; Kingston, P.A.; Manning, T.J.; Conklin, M.W. Outside and in: Development of Neuronal Excitability. *Curr. Opin. Neurobiol.* **2002**, *12*, 315–323. [[CrossRef](#)] [[PubMed](#)]
63. Yasuda, T.; Bartlett, P.F.; Adams, D.J. Kir and Kv Channels Regulate Electrical Properties and Proliferation of Adult Neural Precursor Cells. *Mol. Cell. Neurosci.* **2008**, *37*, 284–297. [[CrossRef](#)] [[PubMed](#)]
64. Srivastava, A.; Das, B.; Yao, A.Y.; Yan, R. Metabotropic Glutamate Receptors in Alzheimer’s Disease Synaptic Dysfunction: Therapeutic Opportunities and Hope for the Future. *J. Alzheimer’s Dis.* **2020**, *78*, 1345–1361. [[CrossRef](#)] [[PubMed](#)]
65. Jurado, S. AMPA Receptor Trafficking in Natural and Pathological Aging. *Front. Mol. Neurosci.* **2018**, *10*, 446. [[CrossRef](#)]
66. Guntupalli, S.; Widagdo, J.; Anggono, V. Amyloid- β -Induced Dysregulation of AMPA Receptor Trafficking. *Neural Plast.* **2016**, *2016*, 3204519. [[CrossRef](#)] [[PubMed](#)]
67. Greenough, M.A.; Lane, D.J.R.; Balez, R.; Anastacio, H.T.D.; Zeng, Z.; Ganio, K.; McDevitt, C.A.; Acevedo, K.; Belaidi, A.A.; Koistinaho, J.; et al. Selective Ferroptosis Vulnerability Due to Familial Alzheimer’s Disease Presenilin Mutations. *Cell Death Differ.* **2022**, *29*, 2123–2136. [[CrossRef](#)] [[PubMed](#)]
68. Lasky, J.L.; Wu, H. Notch Signaling, Brain Development, and Human Disease. *Pediatr. Res.* **2005**, *57*, 104–109. [[CrossRef](#)] [[PubMed](#)]
69. Barbour, A.; Gourmaud, S.; Li, X.; Stewart, D.; Irwin, D.; Talos, D.; Jensen, F. Seizures Exacerbate Excitatory: Inhibitory Imbalance in Alzheimer’s Disease with Attenuation after Rapamycin Treatment in 5XFAD Mice. *bioRxiv* **2023**. [[CrossRef](#)]
70. Guo, C.; Ma, Y.Y. Calcium Permeable-AMPA Receptors and Excitotoxicity in Neurological Disorders. *Front. Neural Circuits* **2021**, *15*, 711564. [[CrossRef](#)]
71. Kawahara, Y.; Ito, K.; Sun, H.; Kanazawa, I.; Kwak, S. Low Editing Efficiency of GluR2 mRNA Is Associated with a Low Relative Abundance of ADAR2 mRNA in White Matter of Normal Human Brain. *Eur. J. Neurosci.* **2003**, *18*, 23–33. [[CrossRef](#)]
72. Wright, A.; Vissel, B. The Essential Role of AMPA Receptor GluA2 Subunit RNA Editing in the Normal and Diseased Brain. *Front. Mol. Neurosci.* **2012**, *5*, 34. [[CrossRef](#)] [[PubMed](#)]
73. Gaisler-Salomon, I.; Kravitz, E.; Feiler, Y.; Safran, M.; Biegon, A.; Amariglio, N.; Rechavi, G. Hippocampus-Specific Deficiency in RNA Editing of GluA2 in Alzheimer’s Disease. *Neurobiol. Aging* **2014**, *35*, 1785–1791. [[CrossRef](#)] [[PubMed](#)]
74. Khermesh, K.; D’Erchia, A.M.; Barak, M.; Annese, A.; Wachtel, C.; Levanon, E.Y.; Picardi, E.; Eisenberg, E. Reduced Levels of Protein Recoding by A-to-I RNA Editing in Alzheimer’s Disease. *RNA* **2016**, *22*, 290–302. [[CrossRef](#)] [[PubMed](#)]
75. Akbarian, S.; Smith, M.A.; Jones, E.G. Editing for an AMPA Receptor Subunit RNA in Prefrontal Cortex and Striatum in Alzheimer’s Disease, Huntington’s Disease and Schizophrenia. *Brain Res.* **1995**, *699*, 297–304. [[CrossRef](#)] [[PubMed](#)]
76. Konen, L.M.; Wright, A.L.; Royle, G.A.; Morris, G.P.; Lau, B.K.; Seow, P.W.; Zinn, R.; Milham, L.T.; Vaughan, C.W.; Vissel, B. A New Mouse Line with Reduced GluA2 Q/R Site RNA Editing Exhibits Loss of Dendritic Spines, Hippocampal CA1-Neuron Loss, Learning and Memory Impairments and NMDA Receptor-Independent Seizure Vulnerability. *Mol. Brain* **2020**, *13*, 27. [[CrossRef](#)] [[PubMed](#)]
77. Pachernegg, S.; Münster, Y.; Muth-Köhne, E.; Fuhrmann, G.; Hollmann, M. GluA2 Is Rapidly Edited at the Q/R Site during Neural Differentiation in Vitro. *Front. Cell. Neurosci.* **2015**, *9*, 69. [[CrossRef](#)] [[PubMed](#)]
78. Lu, W.; Shi, Y.; Jackson, A.C.; Bjorgan, K.; Durning, M.J.; Sprengel, R.; Seeburg, P.H.; Nicoll, R.A. Subunit Composition of Synaptic AMPA Receptors Revealed by a Single-Cell Genetic Approach. *Neuron* **2009**, *62*, 254–268. [[CrossRef](#)] [[PubMed](#)]
79. Wenthold, R.J.; Petralia, R.S.; Blahos, J.; Niedzielski, A.S. Evidence for Multiple AMPA Receptor Complexes in Hippocampal CA1/CA2 Neurons. *J. Neurosci.* **1996**, *16*, 1982–1989. [[CrossRef](#)]
80. Zhang, Q.; Ma, C.; Gearing, M.; Wang, P.G.; Chin, L.S.; Li, L. Integrated Proteomics and Network Analysis Identifies Protein Hubs and Network Alterations in Alzheimer’s Disease. *Acta Neuropathol. Commun.* **2018**, *6*, 19. [[CrossRef](#)]
81. Mendonça, C.F.; Kuras, M.; Nogueira, F.C.S.; Plá, I.; Hortobágyi, T.; Csiba, L.; Palkovits, M.; Renner, É.; Döme, P.; Marko-Varga, G.; et al. Proteomic Signatures of Brain Regions Affected by Tau Pathology in Early and Late Stages of Alzheimer’s Disease. *Neurobiol. Dis.* **2019**, *130*, 104509. [[CrossRef](#)]
82. Johnson, E.C.B.; Dammer, E.B.; Duong, D.M.; Yin, L.; Thambisetty, M.; Troncoso, J.C.; Lah, J.J.; Levey, A.I.; Seyfried, N.T. Deep Proteomic Network Analysis of Alzheimer’s Disease Brain Reveals Alterations in RNA Binding Proteins and RNA Splicing Associated with Disease. *Mol. Neurodegener.* **2018**, *13*, 52. [[CrossRef](#)] [[PubMed](#)]

83. Xu, J.; Patassini, S.; Rustogi, N.; Riba-Garcia, I.; Hale, B.D.; Phillips, A.M.; Waldvogel, H.; Haines, R.; Bradbury, P.; Stevens, A.; et al. Regional Protein Expression in Human Alzheimer's Brain Correlates with Disease Severity. *Commun. Biol.* **2019**, *2*, 43. [[CrossRef](#)] [[PubMed](#)]
84. Yeung, J.H.Y.; Walby, J.L.; Palpagama, T.H.; Turner, C.; Waldvogel, H.J.; Faull, R.L.M.; Kwakowsky, A. Glutamatergic Receptor Expression Changes in the Alzheimer's Disease Hippocampus and Entorhinal Cortex. *Brain Pathol.* **2021**, *31*, e13005. [[CrossRef](#)] [[PubMed](#)]
85. Stepler, K.E.; Mahoney, E.R.; Kofler, J.; Hohman, T.J.; Lopez, O.L.; Robinson, R.A.S. Inclusion of African American/Black Adults in a Pilot Brain Proteomics Study of Alzheimer's Disease. *Neurobiol. Dis.* **2020**, *146*, 105129. [[CrossRef](#)]
86. Sweet, R.A.; MacDonald, M.L.; Kirkwood, C.M.; Ding, Y.; Schempf, T.; Jones-Laughner, J.; Kofler, J.; Ikonovic, M.D.; Lopez, O.L.; Garver, M.E.; et al. Apolipoprotein E*4 (APOE*4) Genotype Is Associated with Altered Levels of Glutamate Signaling Proteins and Synaptic Coexpression Networks in the Prefrontal Cortex in Mild to Moderate Alzheimer Disease. *Mol. Cell. Proteom.* **2016**, *15*, 2252–2262. [[CrossRef](#)] [[PubMed](#)]
87. Johnson, E.C.B.; Carter, E.K.; Dammer, E.B.; Duong, D.M.; Gerasimov, E.S.; Liu, Y.; Liu, J.; Betarbet, R.; Ping, L.; Yin, L.; et al. Large-Scale Deep Multi-Layer Analysis of Alzheimer's Disease Brain Reveals Strong Proteomic Disease-Related Changes Not Observed at the RNA Level. *Nat. Neurosci.* **2022**, *25*, 213–225. [[CrossRef](#)] [[PubMed](#)]
88. Lu, W.; Roche, K.W. Posttranslational Regulation of AMPA Receptor Trafficking and Function. *Curr. Opin. Neurobiol.* **2012**, *22*, 470–479. [[CrossRef](#)] [[PubMed](#)]
89. Roche, K.W.; O'Brien, R.J.; Mammen, A.L.; Bernhardt, J.; Huganir, R.L. Characterization of Multiple Phosphorylation Sites on the AMPA Receptor GluR1 Subunit. *Neuron* **1996**, *16*, 1179–1188. [[CrossRef](#)]
90. Derkach, V.; Barria, A.; Soderling, T.R. Ca²⁺/Calmodulin-Kinase II Enhances Channel Conductance of α -Amino-3-Hydroxy-5-Methyl-4-Isoxazolepropionate Type Glutamate Receptors. *Proc. Natl. Acad. Sci. USA* **1999**, *96*, 3269–3274. [[CrossRef](#)]
91. Banke, T.G.; Bowie, D.; Lee, H.K.; Huganir, R.L.; Schousboe, A.; Traynelis, S.F. Control of GluR1 AMPA Receptor Function by CAMP-Dependent Protein Kinase. *J. Neurosci.* **2000**, *20*, 89–102. [[CrossRef](#)]
92. Fox, C.J.; Russell, K.; Titterness, A.K.; Yu, T.W.; Christie, B.R. Tyrosine Phosphorylation of the GluR2 Subunit Is Required for Long-Term Depression of Synaptic Efficacy in Young Animals in Vivo. *Hippocampus* **2007**, *17*, 600–605. [[CrossRef](#)]
93. Ahmadian, G.; Ju, W.; Liu, L.; Wyszynski, M.; Lee, S.H.; Dunah, A.W.; Taghibiglou, C.; Wang, Y.; Lu, J.; Wong, T.P.; et al. Tyrosine Phosphorylation of GluR2 Is Required for Insulin-Stimulated AMPA Receptor Endocytosis and LTD. *EMBO J.* **2004**, *23*, 1040–1050. [[CrossRef](#)] [[PubMed](#)]
94. Hershko, A.; Ciechanover, A. The Ubiquitin System. *Annu. Rev. Biochem.* **1998**, *67*, 425–479. [[CrossRef](#)]
95. Widagdo, J.; Chai, Y.J.; Ridder, M.C.; Chau, Y.Q.; Johnson, R.C.; Sah, P.; Huganir, R.L.; Anggono, V. Activity-Dependent Ubiquitination of GluA1 and GluA2 Regulates AMPA Receptor Intracellular Sorting and Degradation. *Cell Rep.* **2015**, *10*, 783–795. [[CrossRef](#)]
96. Schwarz, L.A.; Hall, B.J.; Patrick, G.N. Activity-Dependent Ubiquitination of GluA1 Mediates a Distinct AMPA Receptor Endocytosis and Sorting Pathway. *J. Neurosci.* **2010**, *30*, 16718–16729. [[CrossRef](#)] [[PubMed](#)]
97. Widagdo, J.; Guntupalli, S.; Jang, S.E.; Anggono, V. Regulation of AMPA Receptor Trafficking by Protein Ubiquitination. *Front. Mol. Neurosci.* **2017**, *10*, 347. [[CrossRef](#)]
98. Lin, A.; Hou, Q.; Jarzylo, L.; Amato, S.; Gilbert, J.; Shang, F.; Man, H.Y. Nedd4-Mediated AMPA Receptor Ubiquitination Regulates Receptor Turnover and Trafficking. *J. Neurochem.* **2011**, *119*, 27–39. [[CrossRef](#)]
99. Huo, Y.; Khatiri, N.; Hou, Q.; Gilbert, J.; Wang, G.; Man, H.Y. The Deubiquitinating Enzyme USP46 Regulates AMPA Receptor Ubiquitination and Trafficking. *J. Neurochem.* **2015**, *134*, 1067–1080. [[CrossRef](#)] [[PubMed](#)]
100. Lussier, M.P.; Herring, B.E.; Nasu-Nishimura, Y.; Neutzner, A.; Karbowski, M.; Youle, R.J.; Nicoll, R.A.; Roche, K.W. Ubiquitin Ligase RNF167 Regulates AMPA Receptor-Mediated Synaptic Transmission. *Proc. Natl. Acad. Sci. USA* **2012**, *109*, 19426–19431. [[CrossRef](#)]
101. Hayashi, T.; Rumbaugh, G.; Huganir, R.L. Differential Regulation of AMPA Receptor Subunit Trafficking by Palmitoylation of Two Distinct Sites. *Neuron* **2005**, *47*, 709–723. [[CrossRef](#)]
102. Lin, D.T.; Makino, Y.; Sharma, K.; Hayashi, T.; Neve, R.; Takamiya, K.; Huganir, R.L. Regulation of AMPA Receptor Extrasynaptic Insertion by 4.1N, Phosphorylation and Palmitoylation. *Nat. Neurosci.* **2009**, *12*, 879–887. [[CrossRef](#)] [[PubMed](#)]
103. Itoh, M.; Yamashita, M.; Kaneko, M.; Okuno, H.; Abe, M.; Yamazaki, M.; Natsume, R.; Yamada, D.; Kaizuka, T.; Suwa, R.; et al. Deficiency of AMPAR-Palmitoylation Aggravates Seizure Susceptibility. *J. Neurosci.* **2018**, *38*, 10220–10235. [[CrossRef](#)] [[PubMed](#)]
104. Baudry, M.; Massicotte, G.; Hauge, S. Phosphatidylserine Increases the Affinity of the AMPA/Quisqualate Receptor in Rat Brain Membranes. *Behav. Neural Biol.* **1991**, *55*, 137–140. [[CrossRef](#)] [[PubMed](#)]
105. Frank, C.; Rufini, S.; Tancredi, V.; Forcina, R.; Grossi, D.; D'Arcangelo, G. Cholesterol Depletion Inhibits Synaptic Transmission and Synaptic Plasticity in Rat Hippocampus. *Exp. Neurol.* **2008**, *212*, 407–414. [[CrossRef](#)] [[PubMed](#)]
106. Korinek, M.; Gonzalez-Gonzalez, I.M.; Smejkalova, T.; Hajdukovic, D.; Skrenkova, K.; Krusek, J.; Horak, M.; Vyklicky, L. Cholesterol Modulates Presynaptic and Postsynaptic Properties of Excitatory Synaptic Transmission. *Sci. Rep.* **2020**, *10*, 12651. [[CrossRef](#)]
107. Korinek, M.; Vyklicky, V.; Borovska, J.; Lichnerova, K.; Kaniakova, M.; Krausova, B.; Krusek, J.; Balik, A.; Smejkalova, T.; Horak, M.; et al. Cholesterol Modulates Open Probability and Desensitization of NMDA Receptors. *J. Physiol.* **2015**, *593*, 2279–2293. [[CrossRef](#)]

108. Antonini, A.; Caioli, S.; Saba, L.; Vindigni, G.; Biocca, S.; Canu, N.; Zona, C. Membrane Cholesterol Depletion in Cortical Neurons Highlights Altered NMDA Receptor Functionality in a Mouse Model of Amyotrophic Lateral Sclerosis. *Biochim. Biophys. Acta—Mol. Basis Dis.* **2018**, *1864*, 509–519. [[CrossRef](#)]
109. Sanchez-Mejia, R.O.; Newman, J.W.; Toh, S.; Yu, G.-Q.; Zhou, Y.; Halabisky, B.; Cissé, M.; Scearce-Levie, K.; Cheng, I.H.; Gan, L.; et al. Phospholipase A2 Reduction Ameliorates Cognitive Deficits in a Mouse Model of Alzheimer’s Disease. *Nat. Neurosci.* **2008**, *11*, 1311–1318. [[CrossRef](#)]
110. Bernard, J.; Chabot, C.; Gagné, J.; Baudry, M.; Massicotte, G. Melittin Increases AMPA Receptor Affinity in Rat Brain Synaptosomes. *Brain Res.* **1995**, *671*, 195–200. [[CrossRef](#)]
111. Ménard, C.; Patenaude, C.; Massicotte, G. Phosphorylation of AMPA Receptor Subunits Is Differentially Regulated by Phospholipase A2 Inhibitors. *Neurosci. Lett.* **2005**, *389*, 51–56. [[CrossRef](#)]

Disclaimer/Publisher’s Note: The statements, opinions and data contained in all publications are solely those of the individual author(s) and contributor(s) and not of MDPI and/or the editor(s). MDPI and/or the editor(s) disclaim responsibility for any injury to people or property resulting from any ideas, methods, instructions or products referred to in the content.